

# Light Water Reactor Safety Research Program Quarterly Report April - June 1977

Nuclear Fuel Cycle Safety Research Department

Prepared by Sandia Laboratories, Albuquerque, New Mexico 87185  
and Livermore, California 94550 for the United States Nuclear  
Regulatory Commission under DOE Contract AT(29-1)-789

Printed April 1978



Sandia Laboratories

POOR ORIGINAL

POOR

8001100 815

Issued by Sandia Laboratories, operated for the United States  
Department of Energy by Sandia Corporation.

---

#### NOTICE

This report was prepared as an account of work sponsored by the United States Government. Neither the United States nor the United States Department of Energy, nor the United States Nuclear Regulatory Commission, nor any of their employees, nor any of their contractors, subcontractors, or their employees, makes any warranty, express or implied, or assumes any legal liability or responsibility for the accuracy, completeness or usefulness of any information, apparatus, product or process disclosed, or represents that its use would not infringe privately owned rights.

Printed in the United States of America

Available from  
National Technical Information Service  
U. S. Department of Commerce  
5285 Port Royal Road  
Springfield, VA 22161

Price: Printed Copy \$4.50; Microfiche \$3.00

POOR ORIGINAL

SAND77-2060  
NUREG-0183-4  
Unlimited Release  
Printed April 1978

Distribution  
Category R-3

LIGHT WATER REACTOR SAFETY RESEARCH PROGRAM\*  
QUARTERLY REPORT

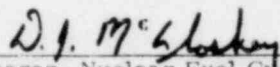
April - June 1977

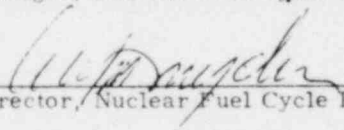
Submitted by

Nuclear Fuel Cycle Safety Research Department  
Sandia Laboratories, Albuquerque, New Mexico 87185

Person in Charge: D. A. Dahlgren

APPROVED:

  
\_\_\_\_\_  
Manager, Nuclear Fuel Cycle Safety Research

  
\_\_\_\_\_  
Director, Nuclear Fuel Cycle Programs

\*This work is supported by the U. S. Nuclear Regulatory Commission  
(Project Numbers A-1019 and A-1030).

## CONTENTS

	<u>Page</u>
1. Molten Core/Concrete Interactions Study	7
1.1 Summary	7
1.2 Small-Scale Melt/Concrete Interaction Tests	8
1.3 Large-Scale Melt/Concrete Interactions	10
1.4 Melt/Concrete Model	13
1.5 Response of Concrete to High-Heat Fluxes	13
2. Steam Explosion Phenomena	18
2.1 Summary	18
2.2 Experimental Apparatus	19
2.3 Instrumentation and Diagnostics	20
2.4 Results of Triggering Experiments	20
2.4.1 Effects of Composition on Steam Explosion Triggering	22
2.4.2 Effect of Water Temperature on the Interaction	24
2.4.3. Effect of the Mode of Pressure Transient Introduction	24
2.5 Debris Analysis	25
2.6 Exploratory Melting Experiments	40
2.7 Containment Breaching Analysis	40
2.8 Steam Explosion Scaling Studies	41
References	43

## ILLUSTRATIONS

<u>Figure</u>		<u>Page</u>
1	Photograph of Containment Fixture Instrumentation	9
2	Photograph of Metal Slug Extracted from Crucible Used in Test LSB-2	12
3	Photograph of Sectioned Metal Slug (Figure 2) after Abrasive Polishing	12
4	Summary of Average Overall Erosion Results	15
5	Variation of Average Overall Erosion Rate with Measured Heat Flux	16
6	Photograph of a Globule of Corium-E Simulant with 59.1 Atom Percent Initial Oxygen Which Had Been Flooded While Molten with $\approx 293$ K Water and Subjected to a Bridgewire Pulse.	23
7	Photograph of a Globule of Corium-E Simulant with 56.4 Atom Percent Initial Oxygen Which Had Been Flooded While Molten with $\approx 293$ K Water and Subjected to a Bridgewire Pulse.	23

ILLUSTRATIONS (Cont'd)

<u>Figure</u>		<u>Page</u>
8	Weights of Various Sieve Fractions for Three Corium-E Samples	26
9	Typical Scanning Electron Micrographs of Sieved Debris from the Interaction of Corium-E Simulant (62.5 Atom Percent Oxygen Initially) Which Had Been Flooded With 295 K Water and Subjected to a Bridge-wire Pulse 0.14 Seconds Later.	28
10	A Scanning Electron Micrograph of a Piece of Sieved Debris from the Interaction of Corium-E Simulant (62.5 Atom Percent Oxygen Initially) Which Had Been Flooded with 295 K Water and Subjected to a Bridge-wire Pulse 0.14 Seconds Later.	29
11	Particles from the Fraction Shown in Figure 9(c).	30
12	Particles from the Fraction Shown in Figure 9(b).	32
13	Scanning Electron Micrographs of As-Retrieved Debris Produced When Molten Corium-E Simulant, 61.5 a/o Initial Oxygen Content, was Flooded with Water and Exposed to a Through-the-Hearth Pressure Transient (9-124-1).	38
14	Photograph of a Cross-Sectioned Sample of Oxidic Corium-A Simulant Which Had Been Arc-Melted and Frozen in Argon (9-131-1).	40
15	Photograph of a Cross-Sectioned Sample of Uranium Dioxide Which Had Been Subjected to Arc Heating and Then Frozen in Argon (9-131-1).	40

TABLES

<u>Table</u>		<u>Page</u>
I	Ideal Melt Compositions	11
II	Summary of Average Overall Erosion Depths	14
III	Summary of Results of Triggering Experiments	21
IV	Corium Simulant Compositions	22
V	Oxidic Corium-E Explosivity as a Function of Initial Oxygen Content	24

LIGHT WATER REACTOR SAFETY RESEARCH PROGRAM  
QUARTERLY REPORT

1. Molten Core/Concrete Interactions Study

1.1 Summary

The Molten Core/Concrete Interactions Study was initiated on July 15, 1975, to provide a qualitative, extensive exploration of the phenomena associated with contact between molten-core materials and concrete. The experimental elements of this study are divided into four categories:

- a. Deposition of Corium-type melts onto concrete.
- b. Kinetics and stoichiometry of the thermal decomposition of concrete.
- c. Response of concrete to high-heat fluxes at one surface.
- d. Simulation experiments that explore phenomena at the interface between a melt and a decomposing solid.

When experimental results have been incorporated in a computer model, a scaling analysis will be made. This will establish scaling parameters for the system and identify key elements of the melt/concrete interaction. A complete project description of the study was issued in December 1975.<sup>1</sup>

During this quarter, development of the small-scale test chamber continued with the addition of instrumentation. Aerosol detectors, gas flow-rate measurements, and gas-phase temperature measurements have been incorporated. These devices will significantly increase the useful data from each test. In addition, a Corium A+R thermite has been successfully developed which includes fission product simulants.

Data reduction and interpretation of the large-scale tests continues. The metal slug used in one of the tests was successfully sectioned, revealing the internal structure and the location of the various melt constituents.

Work on the heat-flux experiments includes a reporting of the measurements of erosion and some preliminary insight into the effects of heating environment on erosion rate. Detailed analysis of the results is well under way and a draft report is essentially complete.

An improved version of the melt/concrete interaction model INTER has been distributed to all known users. Work is progressing on the heat-transfer model for the melt/concrete interface and on the metal oxidation models.

## 1.2 Small-Scale Melt/Concrete Interaction Tests (D. A. Powers)

The containment fixture successfully tested earlier for controlling the interaction between concrete and melts generated metallothermically has been upgraded to include a wide variety of instrumentation. A photograph of the assembly is shown in Figure 1 with a key to the symbols listed in the NOTES. Instrumentation to monitor the nature of the melt/concrete interaction includes:

- a. Acoustic penetration sensors
- b. Concrete temperature sensors
- c. Concrete displacement gages
- d. Aerosol collectors
- e. Aerosol detector
- f. Hygrometer
- g. Gas sampling apparatus
- h. Gas pressure sensors
- i. Gas flow sensors
- j. Sound recorder

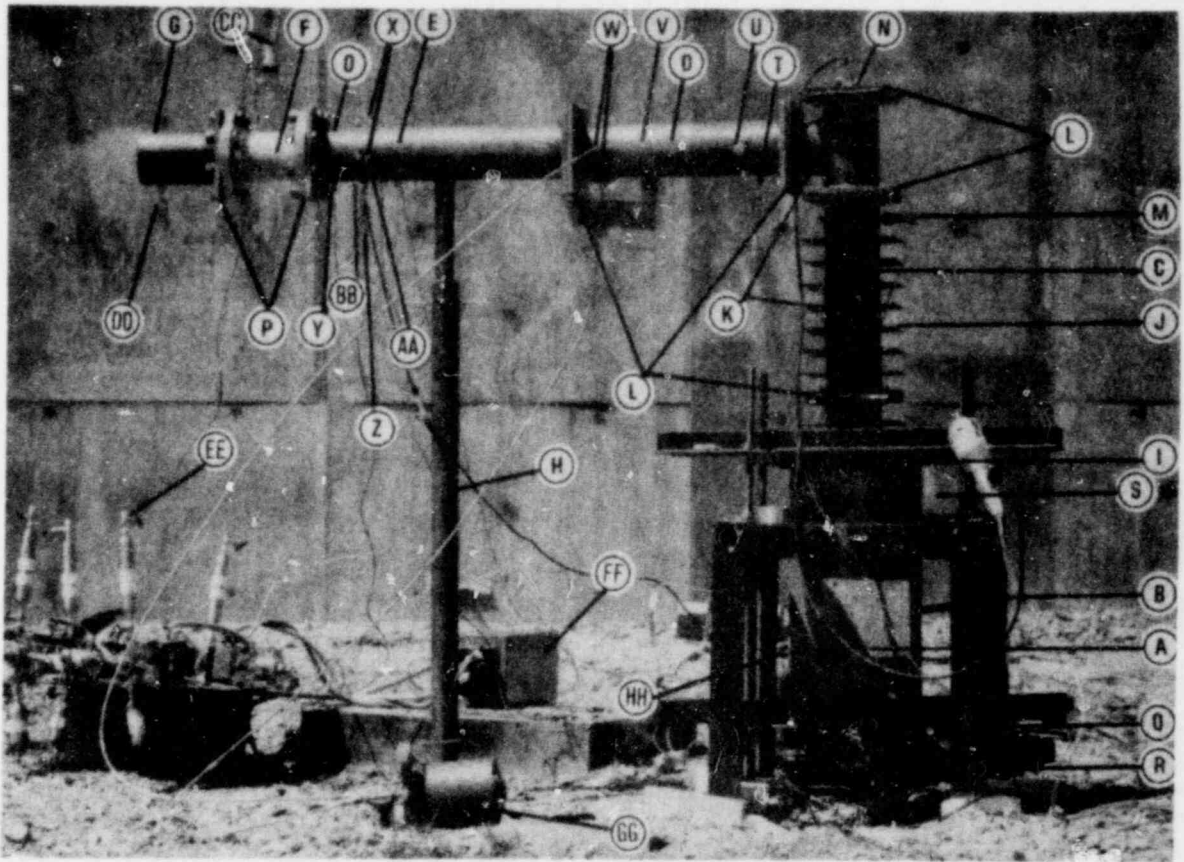
Aerosol collection is based on the aerodynamic diameter of the particulate material. Collection is accomplished by inertial cascade impaction on an eight-stage collector. Size fractionation of this device occurs over the range of about 34 to  $0.5 \mu$ .

Aerosol detection is done by light scattering between an incandescent source and a photovoltaic receiver. Integration of the detection signal and normalization with the aerosol collection results allow aerosol generation rates to be determined.

Gas flow measurements are made by monitoring the pressure drop across a laminar flow element. Clogging of the element is prevented by a Pyrex glass wool total-filter stage immediately in front of the device.

Temperature measurements of the gas stream are monitored by thermocouples. These sensors are equipped with stainless-steel shields to limit radiant heat losses.

The hygrometer was included in the instrumentation because of the difficulty of monitoring the water content of the gas samples extracted during the tests. The device operates on a capacitance principle with an aluminum oxide element. The sensing head is shielded with fritted stainless steel. Other devices in the fixture have been previously described.



NOTES:

- |   |  |
|---|--|
| A. Concrete test crucible                   | R. Embedded thermocouples (6 to 8)               |
| B. Crucible support stand                   | S. Displacement gages (not visible)              |
| C. Cooling tower                            | T. Aerosol carrier gas thermocouple              |
| D. Aerosol sampling chamber                 | U. Aerosol carrier gas pressure transducer       |
| E. Instrumentation chamber                  | V. Cascade impactor aerosol sampler (internal)   |
| F. Laminar flow element                     | W. Connections to aerosol sampler pump           |
| G. Exit vent                                | X. Aerosol detector output and power connections |
| H. Support arm                              | Y. Pressure transducer (not visible)             |
| I. Metal-to-concrete compression seal       | Z. Gas phase thermocouple                        |
| J. Cooling fins                             | AA. Gas sampling port                            |
| K. Bristle baffles (internal)               | BB. Hygrometer (not visible)                     |
| L. Graphite high-temperature seals          | CC. Gas flow differential pressure transducer    |
| M. Blow-out plug                            | DD. Exit gas thermocouple                        |
| N. Ignition assembly and ignition indicator | EE. Gas sampling bottles (13)                    |
| O. Aerosol trap (internal)                  | FF. Gas sampling monitor                         |
| P. Copper gaskets                           | GG. Aerosol sampler pump and associated traps    |
| Q. Acoustic transducers (2)                 | HH. Vacuum pump                                  |

Figure 1. Photograph of Containment Fixture Instrumentation

POOR ORIGINAL



Corium melts to be used in the small-scale experiments have been tested. The reactive mixture has the composition:

U	-----	47.5 w/o
Zr	-----	11.9 w/o
CrO <sub>3</sub>	-----	7.8 w/o
NiO	-----	2.3 w/o
Fe <sub>3</sub> O <sub>4</sub>	-----	23.0 w/o
Type 304 stainless- steel powder	-----	7.5 w/o

The product of reaction has approximately the Corium A+R composition if stoichiometric and complete reaction is assumed:

UO <sub>2</sub>	-----	53.9 w/o
ZrO <sub>2</sub>	-----	16.1 w/o
Stainless steel (18 w/o Cr, 8 w/o Ni, balance Fe)	-----	30.0 w/o

The reaction mixture is also charged with fission product modes. Ideal melt compositions, that is, compositions assuming stoichiometric reactions, are listed in Table I. Strontium and cesium uranates rather than the respective oxides were included in the charge to avoid the hygroscopic and carbon-dioxide-absorbing character of the oxides. The uranates were prepared by firing stoichiometric mixtures of the hydroxides and uranium dioxide (UO<sub>2,2</sub>) in air at 700°C for 24 hrs. The fired mixtures were crushed and refired two additional times.

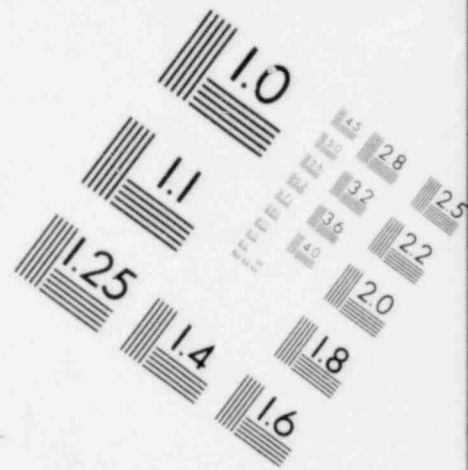
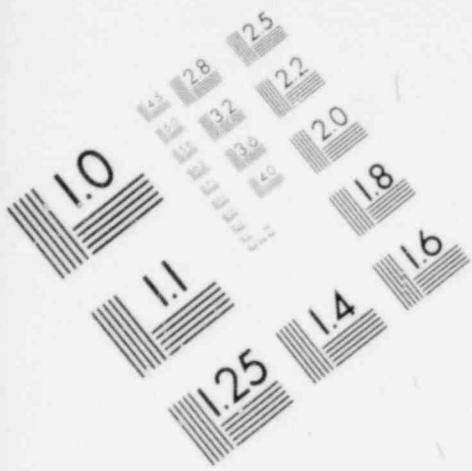
### 1.3 Large-Scale Melt/Concrete Interactions (D. A. Powers)

A metal slug extracted from the crucible used in test LSB-2 is shown in Figure 2. This slug was cut, with much difficulty, to show the internal structure of the solidified metal. This sectioned metal after abrasive polishing is shown in Figure 3. The metal is compact at the bottom with few voids or inclusions. Voids appear in the metal about midplane of the slug and become progressively more numerous toward the top of the slug. Inclusions which appear to be solidified slag are found primarily only in the top 2 in. of the metal. These inclusions were the source of difficulties encountered in cutting the metal. These inclusions suggest that the surface of the melt was vigorously agitated during solidification, but the dramatic density differences between slag and metal prevented extensive mixing of the two phases. Were the slag composed of more dense constituents, such as Cr<sub>2</sub>O<sub>3</sub> or UO<sub>2</sub>, more intimate mixing might have occurred.

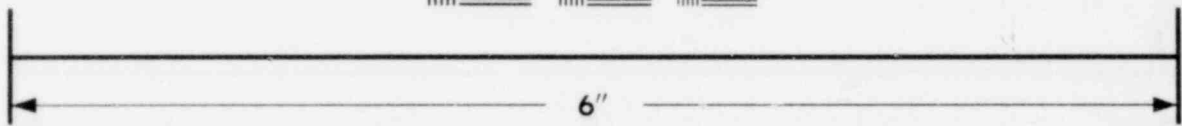
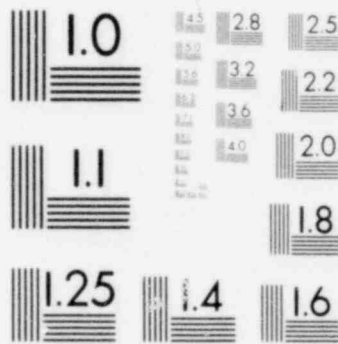
The cross section shown in Figure 3 demonstrates the inadequacy of making small incisions or drillings to determine the quality of solidified melts. The complexities of the structure are typically deep within the metal while metal near the surfaces of the slug is fairly compact.

TABLE I  
Ideal Melt Compositions

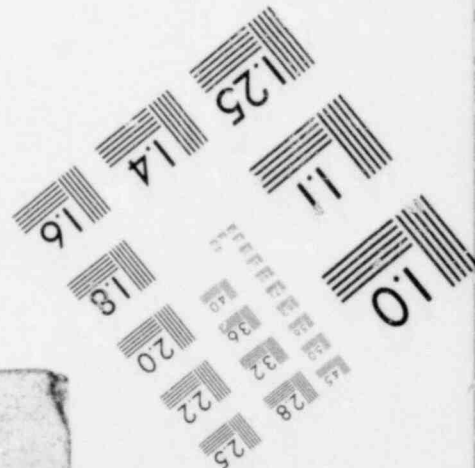
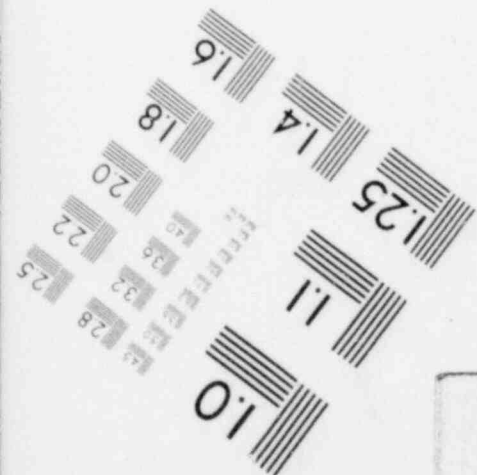
<u>Species</u>	<u>Steel Melt</u>	<u>Corium Melt</u>
UO <sub>2</sub>	2.11	51.8
ZrO <sub>2</sub>	0.92	15.48
Cr	0	5.4
Fe	51.0	22.2
Ni	0	2.4
Al <sub>2</sub> O <sub>3</sub>	41.3	0.0
SrO	0.36	0.66
Cs <sub>2</sub> O	0.32	0.21
MoO <sub>3</sub>	1.05	0.72
CeO <sub>2</sub>	0.92	0.64
La <sub>2</sub> O <sub>3</sub>	0.92	0.64
SnO <sub>2</sub>	0.92	0.64



**IMAGE EVALUATION  
TEST TARGET (MT-3)**



**MICROCOPY RESOLUTION TEST CHART**



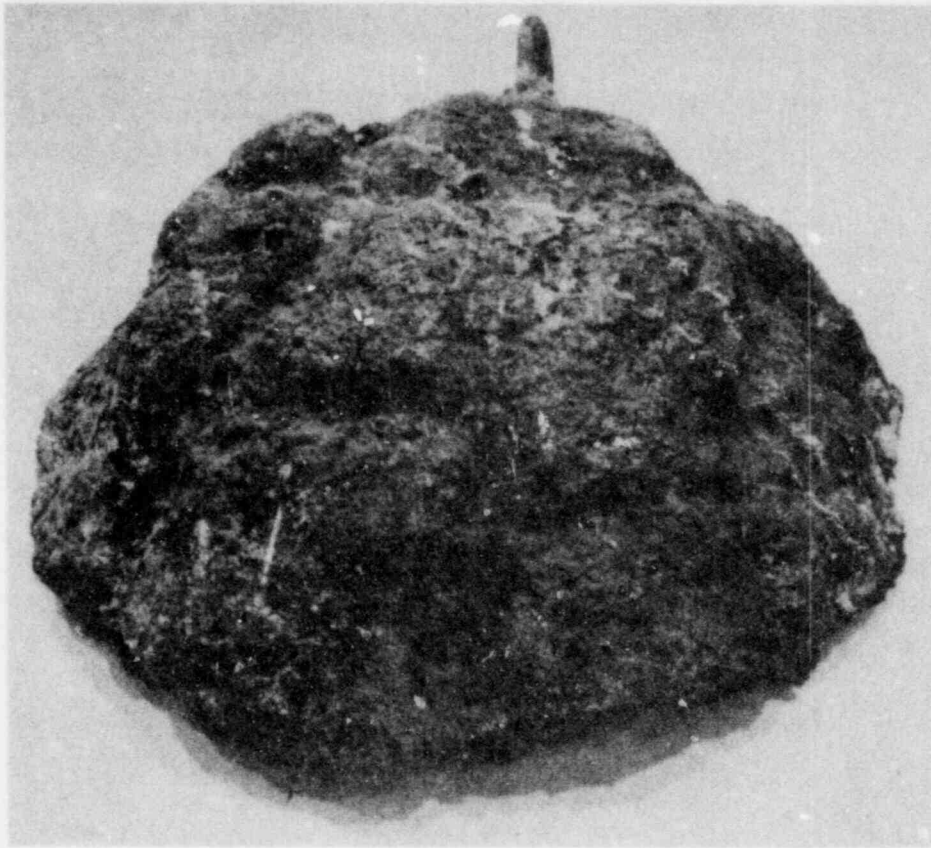


Figure 2. Photograph of Metal Slug Extracted from Crucible Used in Test LSB-2

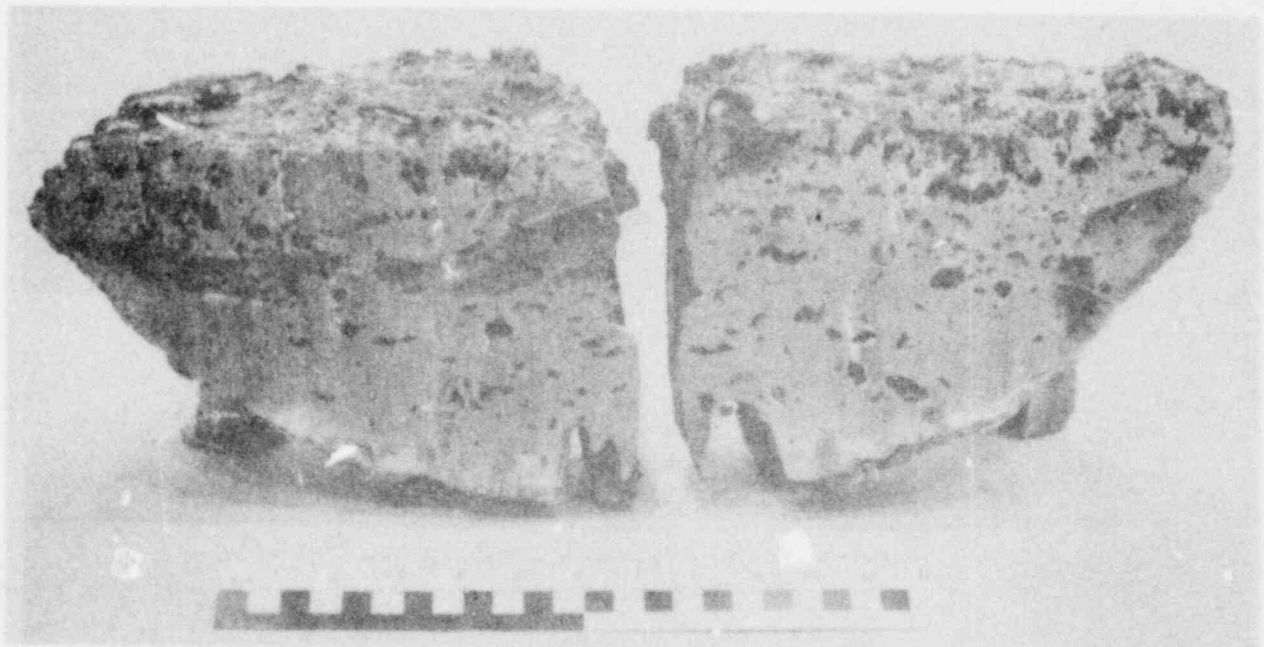


Figure 3. Photograph of Sectioned Metal Slug (Figure 2) after Abrasive Polishing

#### 1.4 Melt/Concrete Model (W. B. Murfin)

A new version of the INTER code, designated INTER1, has been distributed to all users. This version corrects some programming errors that had been made in the previous version; however, the model is similar to that previously reported. This version has been extensively exercised in a study of containment meltthrough for both PWR's and BWR's.

A need has been seen to include some alternate heat-transfer models in addition to the empirical model currently employed. Models being investigated include a vapor film model based on Berenson's film boiling analysis and a discrete bubble model. It would also be useful to revise the gas/metal reaction model. The oxidation of iron and nickel should be dependent on the  $H_2/H_2O$  ratio. This dependence is not specifically included; however, the system of reaction preferences in the model suppresses the oxidation of nickel when Zr and Cr are being oxidized, at which time the  $H_2/H_2O$  ratio is high. Thus nickel oxidation is somewhat slowed. However, the rate of iron oxidation is too high and should be similarly suppressed.

It would also be helpful to users to be able to determine rationally the proper time step. Because of the extreme nonlinearity of the code, this will have to be based on numerical experiments.

#### 1.5 Response of Concrete to High-Heat Fluxes (J. F. Muir)

The response of concrete to severe thermal attack on one surface is studied while uncoupled from the overall molten core/concrete interaction situation. Primary emphasis is on defining the mechanism and rate of surface erosion, and the effects thereon of aggregate material and size, heating environment, material removal mechanism, and conduction of heat into the concrete through exposed reinforcing rods. Activity since the last report focused on completion of the posttest surface erosion measurements and reduction, plotting, and analysis of the data.

Micrometer measurements were made on 16 of the 19 plasma-jet test samples and on 9 out of the 12 radiant-heat test samples to determine eroded surface profiles and the overall erosion of the concrete. Hydration and carboxylation of the limestone samples following the tests caused the initially hard eroded surfaces to turn to a soft powder to a depth varying from about 0.3 to 2.0 cm below the original posttest profiles. Also during the posttest period, the solidified melt layer covering the surfaces of the basalt samples tested in the radiant heat facility loosened and, in most cases, fell away or could be easily removed from the samples. As a result, surface erosion measurements were made, where possible, both before and after these occurrences. For simplicity, both types of occurrences will be referred to as "hydration" and the erosion data designated as either "before hydration" or "after hydration". In those instances where neither phenomenon occurred (i. e., for the basaltic samples tested in the plasma-jet) the erosion data are designated "no hydration". When surface degradation did occur, all loose material was scraped off the samples with a blunt instrument prior to making the "after hydration" measurements.

Average overall erosion depths were determined from the posttest erosion data for each set of profiles (i. e., "before hydration", "after hydration", or "no hydration") for each sample for which posttest measurements were made. This was accomplished by folding the various profiles of each set about the sample centerline and superimposing them on each other along one radius. The average value for the set was subsequently determined by passing a straight line through an appropriate portion of the profile and perpendicular to the sample centerline. For the plasma-jet samples, the portion selected was the relatively flat region on top of the central hump (i. e., in the stagnation region of the jet), while for the radiant-heat samples, as much of the eroded surface as possible was selected. The results are summarized in Table II (no average erosion depths were obtained for the samples containing reinforcing rod). The uncertainty in the average overall surface erosion depth is estimated to be the greater of  $\pm 0.05$  cm or  $\pm 5\%$  for all samples tested.

TABLE II  
Summary of Average Overall Erosion Depths

Test-Sample No.	Type of Concrete	Average Measured Heat Flux (W/cm <sup>2</sup> )	Test Time (min)	Average Erosion (cm)	
				No Hydration or Before Hydration	After Hydration
P3-14	L, F	243	2.42	1.67	1.81
P5-18	L, F	121	3.58	—*	0.93
P6-35	B, F	274	2.75	2.30	—**
P7-28	B, C	121	3.90	0.90	—**
P9-10	L, C	120	3.40	0.41	0.84
P10-19	L, F	270	1.77	1.19	1.28
P11-34	B, F	124	3.43	0.64	—**
P12-27	B, C	275	1.78	1.78	—**
P13-11	L, C	291	1.77	1.38	1.55
P14-20	L, F	134	2.07	0.10	0.50
P18-29	B, F	302	1.05	1.17	—**
P19-30	B, F	233	1.73	2.03	—**
RH2-6	L, C	116	5.19	—*	1.93
RH3-15	L, F	118	3.86	—*	1.40
RH4-25	B, C	105	8.33	—*	2.22
RH7-4	L, C	105	8.56	2.66	3.07
RH8-31	B, F	104	8.05	2.23	2.50
RH10-26	B, C	104	11.17	2.13	2.51
RH11-16	L, F	32	59.8	-0.11	1.74
RH12-32	B, F	64	29.8	3.19	4.00

\* Hydration occurred and surface crumbled prior to making "Before Hydration" measurements.

\*\* No Hydration occurred.

L - Limestone, B - Basalt, F - Fine, C - Coarse

A clearer insight into the dependence of concrete erosion on heat-flux level is provided by Figure 4 which presents the tabulated average overall erosion depths as a function of test time, average measured heat flux (determined from calorimeter data), aggregate material and size, and test facility. The dashed lines, which represent constant erosion rates, were drawn so as to generally bracket the "no hydration" or "before hydration" results for the four nominal heating conditions. Except for the two lowest heating conditions (at which there was only one test each), the results generally lie within the boundaries indicated. The two most noticeable exceptions to this are the values for the plasma-jet test samples P9-10 and P14-20. Both of these samples experienced very little erosion. Since the average erosion before hydration amounted to no more than 0.16 and 0.10, respectively, of the maximum aggregate dimension, they are probably not representative of the long-term behavior of each concrete during ablation to depths of the order of, or several times, the characteristic aggregate dimension.

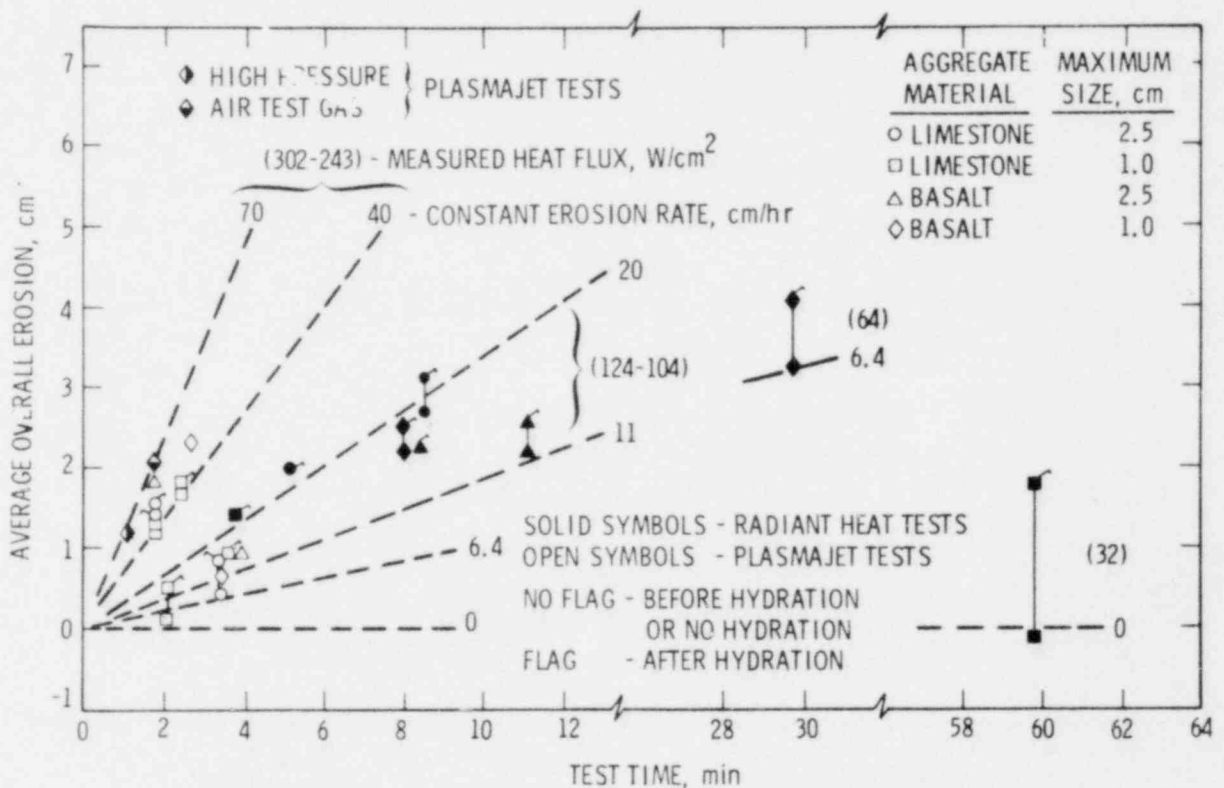


Figure 4. Summary of Average Overall Erosion Results

The overall erosion obtained during the tests ranged from essentially zero (at the lowest heat flux condition)<sup>1</sup> to a maximum of about 3 cm (before hydration) with the bulk of the data falling between about 1 and 3 cm. The corresponding constant erosion rates are seen to vary from zero to a maximum of approximately 70 cm/hr, and exhibit a trend of increasing erosion rate with heat flux.

<sup>1</sup> No appreciable melting or erosion of the concrete was experienced during the hour-long radiant heat test at this heating condition.<sup>2</sup>

Average overall erosion rates were computed from the posttest surface erosion data by dividing the "no hydration" and "before hydration" average erosion depths by the corresponding test time (i. e., the values in columns 5 and 4 of Table II, respectively). In the case of the four test samples for which hydration and surface crumbling occurred before any surface erosion measurements were made, average "before hydration" depths were estimated based on the "after hydration" measurements for these samples and differences between the "before" and "after hydration" measurements for like samples exposed to similar heating conditions.

These results are presented in Figure 5 versus the average measured heat fluxes. The latter are indicative of the heating environments provided by the facilities rather than the heat fluxes into the concrete samples. Erosion rates are presented for all but test samples P9-10 and P14-20 for which the ratios of average erosion to maximum aggregate dimension are too small for the results to be considered meaningful. The dashed lines enclosing the data are included to illustrate the trend of increasing erosion rate with heat flux noted above and to indicate the overall scatter in the results (from approximately 15 to 25 cm/hr).

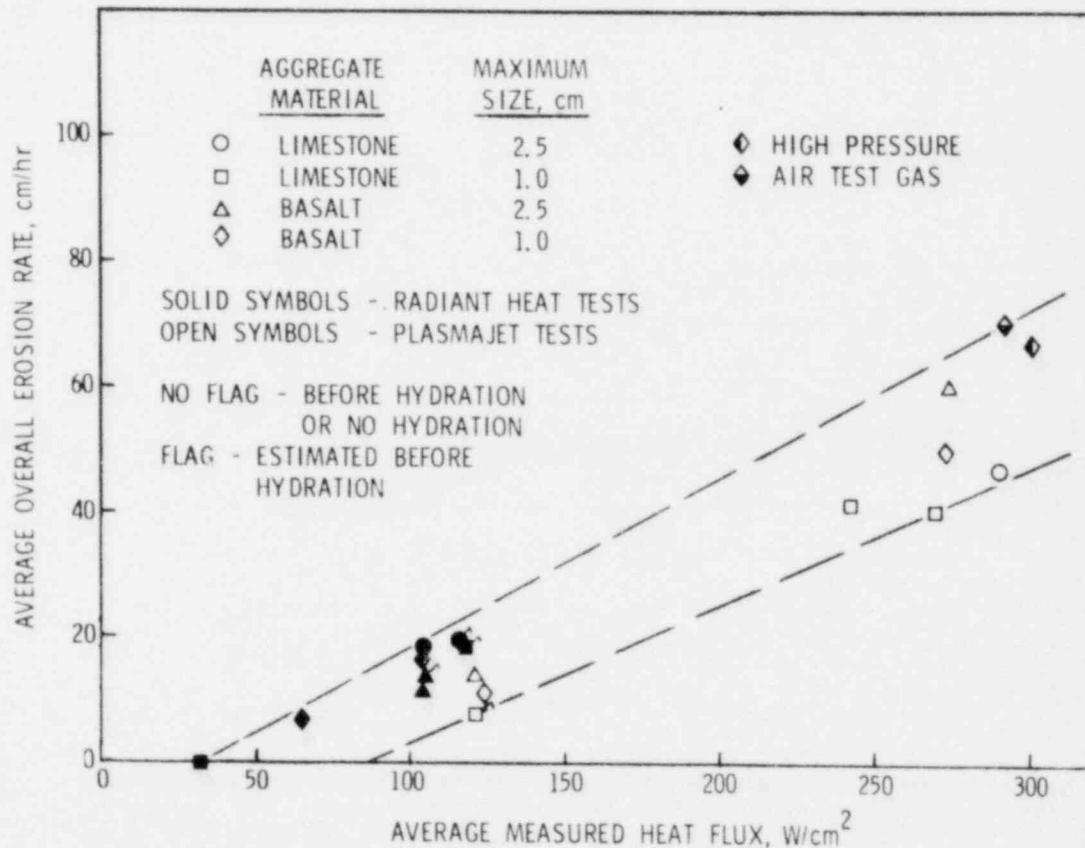


Figure 5 Variation of Average Overall Erosion Rate with Measured Heat Flux



Since differences between the points for the two facilities and for the different concrete types are of the same order as the uncertainties in the results, the effects of heating environment and aggregate material and size on erosion rate cannot be evaluated from these results.

Attention is directed to the fact that the above results are applicable only to the conditions and environments of the present experiments (detailed descriptions of which are contained in previous quarterly reports 1-4). Extrapolation to other situations outside the regimes of the experiments should be undertaken with considerable caution.

Analyses of the net heat fluxes to the melting concrete surfaces and of the in-depth temperature data are almost complete. A comprehensive topical report on the concrete heat-transfer experiments is in draft form.

## 2. Steam Explosion Phenomena (L. S. Nelson and L. D. Buxton)

### 2.1 Summary

A summary of the primary accomplishments during this quarter is given below:

- a. The parametric variations initiated last quarter with "oxidic" Corium-E simulant triggering experiments were continued this quarter, as follows:
  - (i) The effects of initial composition of the oxide melt on steam-explosion triggering were studied further as a function of the initial atom percent of oxygen, holding the iron:zirconium:uranium atom ratio constant. In the previous quarter,<sup>5</sup> compositions with 62.5 atom percent and 61.5 atom percent initial oxygen gave rise to steam explosions, fine fragmentations, and interaction-generated pressure pulses with high probability. Melts which initially contained only 53.2 atom percent oxygen did not show steam explosion triggering activity. In this quarter, we studied two compositions intermediate between these, 59.1 and 56.4 atom percent initial oxygen. The material with 59.1 atom percent showed fine breakup and produced mild pressure pulses, while the 56.4 atom percent oxygen material fragmented in only one experiment out of seven and never yielded an interaction-generated pressurization.
  - (ii) The effect of increased water temperature was studied by flooding the known explosive, 61.5 initial atom percent oxygen-containing Corium-E simulant, with 333 to 343 K water. No explosion or fragmentation could be detected. However, it is not certain whether the melts were of sufficiently high temperature. Also, with the increased water temperature, the mechanics of flooding were slightly different and the boiling films would be expected to be thicker.
  - (iii) The effect of the mode of pressure transient introduction was studied further by use of the beneath-the-earth detonator-projectile combination. Several samples of the 61.5 initial atom percent oxygen-containing Corium-E simulant were flooded with  $\approx 293$  K water and the pulse from the projectile applied at times bracketing the time of suspected greatest explosivity during the flooding. No explosions or fragmentation were recorded in these experiments.
- b. Debris analysis was continued on one of the specimens reported on previously<sup>5</sup> which exploded (62.5 initial atom percent oxygen-containing Corium-E simulant). It was shown

that the finer sieve fractions contain mostly the nonspheroidal debris, the intermediate size fragments are mostly spheroidal, and the largest fragments are jagged and often nonmelted material.

- c. Some exploratory melting experiments were performed with fully oxidic Corium-A, both in the Centorr and the floodable arc-melting apparatus. Melting in argon and subsequent cooling were performed, but flooding was not attempted. In addition, uranium dioxide was subjected to the conditions of arc-melting. The melting was poor, with considerable vaporization and wall deposition. The uranium dioxide behaved much like the metallic Corium-E reported previously.
- d. Several triggering experiment apparatus improvements were worked on. These include installing the new hot water system, doing further work with the projectile-minidetector pressure transient generator, and experimentation with time encoding of the tape deck and high-speed camera records.
- e. Preliminary analyses of containment breaching by steam-explosion generated missiles were performed during the quarter. Both large missiles (such as the reactor vessel head) and small missiles (such as pipes and rods) were considered. There were no indications in the analyses that such missiles could not penetrate the containment, but the analyses were admittedly fraught with uncertainties.
- f. Two papers on steam-explosion triggering were presented at the American Nuclear Society 1977 annual meeting in New York.<sup>6, 7</sup> A rough draft of a document on the need and scope of scaling experiments was submitted to the Fuel Behavior Research Branch, Office of Nuclear Regulatory Research, U.S. Nuclear Regulatory Commission for comment.<sup>8</sup>

## 2.2 Experimental Apparatus

Improvements were made on the upward-driven projectile apparatus discussed briefly in the previous quarterly report.<sup>5</sup> These consisted mainly of improvements in the mode of recording velocity information for the projectile. In that regard, a dual-beam, dual-time-base oscilloscope was installed to record the wire-clipping information.

A hot water system was installed to allow higher temperature water for the triggering experiments. The hot water system consisted of a 1650-W, 6-gal-capacity hot water heater, a circulating pump, and a pair of solenoid valves in both the inlet and outlet lines to the outer chamber of the arc melting/flooding apparatus. In use, the water is brought to a predetermined temperature and just prior to the experiment is circulated through the outer chamber of the arc melting/flooding apparatus. A few tenths of a second prior to sleeve release, the solenoid valves in both the inlet

and outlet lines are closed off; afterward, water is no longer circulated, in order to preserve the debris which may form. Using this system, it has been possible to flood the melts with 333 to 343 K water.

The hot water system was built with a simple water overflow outlet standpipe in the outer chamber to adjust the maximum water level. The height of the standpipe was chosen to achieve a flooding water volume identical to that of the previous cold water experiments. Unfortunately, the standpipe used did not have sufficient capacity to carry the excess water away rapidly enough. Instead, the hot water actually filled the outer chamber completely, with the circulation then being controlled by the pump pressure. Consequently, the flooding for the hot water experiments was perhaps different from that for the cold water experiments because of both the larger total quantity of water involved and the possibility of a slightly elevated system pressure. This is in addition, of course, to any possible differences caused by changed film boiling characteristics as the water temperature increased.

### 2.3 Instrumentation and Diagnostics

Effort was initiated this quarter on setting up an Ampex high-speed (120 ips), 14-channel, FM magnetic tape deck for simultaneous recording of various data associated with the steam-explosion triggering experiments. The data are ultimately intended to include the pyrometer and thermocouple output, pressurization signals from the multiple lithium niobate transducers, and initialization pulses from the transient generator circuit. In addition to the experimental data, a common time code is to be applied to one channel of the tape record using an IRIG-A time code generator. The generator to be used produces both a modulated 10-kHz sine wave signal for FM tape recording and a train of dc pulses containing the same information. The train of dc pulses can be used to drive a light-emitting diode (LED) in the high-speed camera which will thus encode the film edge. The time code application to both types of records allows absolute time cross referencing of all data. The system is not yet implemented completely because of signal conditioning problems.

Further exploration of the possible use of high-speed digital oscilloscopes was also carried out this quarter.

### 2.4 Results of Triggering Experiments

As in previous quarterly reports, the results of the individual steam-explosion triggering experiments are presented in Table III. This is a summary of all experiments done during this quarter.

TABLE III  
Summary of Results of Triggering Experiments

Material	Expt. No.	Sample Weight (g)	Water Temp. (K)	Water Amount (cc)	Melt Atm.	Melt Temp. (K)	Transient Generator	Delay Time (s)	Flash X-Ray	High-Speed Photo (ft)	Remarks
Oxidic Corium-E <sup>a</sup>	9-125-1	15.12	293.4	1500	Ar	2007	THPROJ	0.207	Three pulse	400	Sample intact, with large caldera.
Oxidic Corium-E <sup>a</sup>	9-126-5	15.09	286.7	1500	Ar	2034	THPROJ	0.203	Three pulse	400	Same as 9-125-1
Oxidic Corium-E <sup>a</sup>	9-128-2	15.22	Not recorded	1500	Ar	1976	THPROJ	0.186	None	400	Same as 9-125-1
Oxidic Corium-E <sup>a</sup>	9-129-1	15.17	290.2	1500	Ar	1931	THPROJ	0.051 <sup>e</sup>	None	400	Same as 9-125-1
Oxidic Corium-E <sup>a</sup>	9-129-2	15.14	293.0	1500	Ar	2089	THPROJ	0.272	None	400	Same as 9-125-1
Oxidic Corium-E <sup>a</sup>	9-130-1	15.00	288.1	1500	Ar	2040	BW	0.210	Three pulse	400	Residue resembled mud. Gave 0.7 MPa pulse 5.2 ms after transient.
Oxidic Corium-E <sup>b</sup>	9-134-1	15.41	291.1	1500	Ar	1988	BW	0.138	Three pulse	400	Residue is spheroidal powder. Small pulse 0.5 ms after transient.
Oxidic Corium-E <sup>b</sup>	9-134-2	15.44	290.4	1500	Ar	1941	BW	0.25 <sup>f</sup>	Three pulse	400 <sup>f</sup>	Residue is a fine powder. Small pulses 0.5, 5.5 ms after transient.
Oxidic Corium-E <sup>b</sup>	9-135-1	15.43	298.2	1500	Ar	1979	None	--	Three pulse	400	Control. One piece sample with cavity and bulge.
Oxidic Corium-E <sup>b</sup>	9-135-2	15.43	291.1	1500	Ar	Not recorded	BW	0.200	Three pulse	400	Convex globule. Arcs extinguished before flooding.
Oxidic Corium-E <sup>b</sup>	9-135-3	15.42	291.0	1500	Ar	1955	BW	0.193	Three pulse	400	Residue is a powder with some tiny spheres. Small pulses: 0.5 MPa 1.8 ms after transient, and 0.4 MPa 5.5 ms after transient.
Oxidic Corium-E <sup>b</sup>	9-136-1	15.42	291.2	1500	Ar	1801	BW	0.261	Three pulse	400	Residue is a powder with some angular chunks. 0.2 MPa pulse 1 ms after transient.
Oxidic Corium-E <sup>b</sup>	9-136-2	15.43	292.1	1500	Ar	1680	BW	0.339	Three pulse	400	Sample appeared cool on film. One-piece sample with many voids.
Oxidic Corium-E <sup>c</sup>	9-136-3	15.17	294.0	1500	Ar	1794	BW	0.158	Three pulse	400	Residue is a powder. Broad 0.2 MPa pulse 1 ms after transient.
Oxidic Corium-E <sup>c</sup>	9-137-1	15.27	298.1	1500	Ar	2102	BW	0.214	Three pulse	400	One-piece sample with bulge and cavity.
Oxidic Corium-E <sup>c</sup>	9-137-2	15.27	293.5	1500	Ar	2147	BW	0.263	Three pulse	400	Similar to 9-137-1
Oxidic Corium-E <sup>c</sup>	9-138-1	15.25	295.7	1500	Ar	2052	BW	0.216	Three pulse	400	Similar to 9-137-1
Oxidic Corium-E <sup>c</sup>	9-138-2	15.30	301.6	1500	Ar	2054	BW	0.159	Three pulse	400	Coarse fragmentation, many hollow particles
Oxidic Corium-E <sup>c</sup>	9-142-1	15.22	293.1	1500	Ar	1855	BW	0.146	Three pulse	400	Similar to 9-137-1
Oxidic Corium-E <sup>c</sup>	9-142-2	15.15	292.9	1500	Ar	1850	BW	0.146	Malfunction	400	Similar to 9-137-1. Film shows several small globules of melt in film boiling "bags"
Oxidic Corium-E <sup>d</sup>	9-138-3	16.88	336.2	2524	Ar	Not recorded	BW	0.165	Three pulse	400	Flat, one-piece sample with 10 x 15 mm cavity, a few spherules.
Oxidic Corium-E <sup>d</sup>	9-139-1	18.42	337.0	2524	Ar	1869	BW	0.191	Three pulse	400	Coarse fragmentation. Film shows globules in film boiling "bags".
Oxidic Corium-E <sup>d</sup>	9-140-1	21.12	347.8	2524	Ar	1716	BW	0.157	Three pulse	400	Convex one-piece sample probably frozen at flooding time.
Oxidic Corium-E <sup>d</sup>	9-140-2	18.25	339.3	2524	Ar	1772	BW	0.216	Three pulse	400	One-piece sample with a little coarse fragmentation.
Oxidic Corium-E <sup>d</sup>	9-141-1	17.24	337.4	2524	Ar	1711	BW	0.158	Three pulse	400	Sample broken into many pieces, with a few spherules.
Oxidic Corium-E <sup>d</sup>	9-142-3	15.30	347.2	2524	Ar	1432	BW	0.127	Three pulse	400	One-piece sample with a caldera.
Oxidic Corium-E <sup>d</sup>	9-143-1	15.34	338.2	2524	Ar	1845	BW	0.159	Malfunction	400	Sample damaged during retrieval. Essentially one-piece.
Oxidic Corium-A <sup>d</sup>	9-127-1	14.94	--	Not flooded	Ar	Not recorded	None	None	None	None	Melted in ventorr apparatus.
Oxidic Corium-A <sup>d</sup>	9-131-1	15.02	--	Not flooded	Ar	Not recorded	None	None	None	None	Melted in floodable arc melter.
DO <sub>2</sub>	9-131-2	~10	--	Not flooded	Ar	Not recorded	None	None	None	None	Melted in floodable arc melter. Much vaporization.

<sup>a</sup>Initial oxygen content was 61.5 %O. See Table II.

<sup>b</sup>Initial oxygen content was 59.1 %O. See Table IV.

<sup>c</sup>Initial oxygen content was 56.4 %O. See Table IV.

<sup>d</sup>Initial oxygen content was 64.2 %O. See Table IV.

<sup>e</sup>Could not identify pressure transient on film. Used projectile travel time of 9.4 ms determined independently.

<sup>f</sup>No timing on film. Delay estimated from apparatus settings.

BW = bridgewise exploded in the water.

THPROJ = through-the-hearth pulse generated by striking the stainless-steel projection beneath the hearth with a miniature-air-driven projectile.

POOR ORIGINAL

### 2.4.1 Effects of Composition on Steam-Explosion Triggering

To extend the work on the effect of the initial oxygen content of the Corium-E simulants which was reported last quarter, two new intermediate compositions have been studied, both interacted with 283 to 303 K water. The compositions of all the various Corium-E simulants used to date are summarized in Table IV.

TABLE IV  
Corium Simulant Compositions

Composition	Weight Percent						Total Atom Percent				Metal Atom Percent		
	U <sub>3</sub> O <sub>8</sub>	UO <sub>2</sub>	Zr	ZrO <sub>2</sub>	Fe	Fe <sub>2</sub> O <sub>3</sub>	U	O	Zr	Fe	U	Zr	Fe
Metallic Corium-E*	--	35.0	10.0	--	55	--	8.74	17.49	7.39	66.39	10.59	8.95	81.46
Oxidic Corium-E with 62.5 a/o oxygen	28.3	--	--	10.5	--	61.4	3.96	62.51	3.34	30.19	10.55	8.92	80.52
Oxidic Corium-E with 61.5 a/o oxygen	--	27.6	--	10.7	--	61.8	4.09	61.51	3.47	30.94	10.61	9.01	80.37
Oxidic Corium E with 59.1 a/o oxygen	--	28.2	--	10.9	5.6	55.2	4.34	59.10	3.68	37.89	10.60	8.99	80.40
Oxidic Corium-E with 56.4 a/o oxygen	--	28.9	--	11.2	11.5	48.4	4.62	56.37	3.93	35.08	10.59	9.00	80.40
Oxidic Corium-E with 53.2 a/o oxygen	--	29.7	--	11.5	17.8	41.0	4.97	53.80	4.22	37.62	10.62	9.01	80.37
Metallic Corium-A	--	65.0	18.0	--	17.0	--	19.7	39.3	16.1	24.9	32.4	26.6	41.0
Oxidic Corium-A with 64.2 a/o oxygen	--	57.3	--	21.4	--	21.4	11.6	64.2	9.5	14.7	32.4	26.6	41.0

\* Composition simplified from Reference 9.

Seven experiments (numbers 9-134-1 through 9-136-2 in Table III) were performed with material which initially contained 59.1 atom percent oxygen. The samples were flooded and subjected to a bridgewire pulse under known explosive conditions for the more highly oxidized corium-E simulants as described previously.<sup>5, 10</sup> Three experiments showed no breakup or appreciable interaction between the melt and the water. A typical unfragmented globule of this composition is shown in Figure 6. Four out of the seven experiments, however, yielded fragmentation and generated second-stage pressure pulses, although these pulses were small compared with those produced with the more oxidic Corium-E simulants. The fragmentation was extensive and the particle sizes are thought to be small, but no analyses or sieve separations have been performed as yet on these samples.

A similar series of seven experiments (numbers 9-136-3 through 9-142-2 in Table III) was performed with an oxidic Corium-E simulant which initially contained 56.4 atom percent of oxygen. The material was melted and interacted with 283 to 303 K water, again under the known explosive conditions. With this composition, six experiments yielded unfragmented globules such as the one shown in Figure 7; only one of the seven experiments produced significant fragmentation and in this experiment there was no detectable interaction-generated pressure pulse which might be associated with a second-stage interaction. There was, however, a small broad pulse observed soon after the firing of the bridgewire, similar to those frequently seen preceding the second-stage pulse. The film record of this experiment also indicated the occurrence of only a single stage for the interaction.



Figure 6. Photograph of a Globule of Corium-E Simulant with 59.1 Atom Percent Initial Oxygen Which Had Been Flooded While Molten with  $\approx 293$  K Water and Subjected to a Bridgewire Pulse. Sample did not fragment (9-136-2). Grid is 6.4 mm.



Figure 7. Photograph of a Globule of Corium-E Simulant with 56.4 Atom Percent Initial Oxygen Which Had Been Flooded While Molten with  $\approx 293$  K Water and Subjected to a Bridgewire Pulse. Sample did not fragment (9-137-2). Grid is 6.4 mm.

The results of all the experiments with Corium-E simulants of various initial oxygen contents have been summarized in Table V. The important feature to note is that the tendency to undergo steam-explosion triggering seems to decrease as the initial oxygen content in the melt decreases. This is the trend expected if the impulse-initiated gas release theory<sup>7</sup> is valid for the initial fragmentation event.

POOR ORIGINAL

TABLE V

Oxidic Corium-E Explosivity as a Function of Initial Oxygen Content

<u>Initial Atom Percent Oxygen</u>	<u>Observation</u>
62.5	Violent explosion
61.5	Violent explosion
59.1	Mild explosion
56.4	Slight explosion
53.2	Inert
17.5	Inert (limited data base)

#### 2.4.2 Effect of Water Temperature on the Interaction

Here, the new hot water circulating system described earlier was used to produce 333 to 343 K water in the outer chamber of the reaction vessel prior to flooding. A series of seven hot-water experiments (numbers 9-138-3 through 1-143-1 in Table III) was performed. The Corium-E simulant used was one known to be explosive with cold water for the applied transients used. Only very coarse fragmentation was observed for the most vigorous of these experiments. No pressurizations occurred, and some of the samples remained completely intact.

Besides the earlier mentioned problems with the hot water system, another characteristic of this sequence of experiments is that the pyrometer readings just prior to flooding were all low: less than 1873 K. Prior to these experiments, the copper hearth had built up some black deposits which may have been interfering with electrical conduction and/or heat transfer to the hearth and thus may have changed the properties of the melt. Several more experiments are planned in which the temperature of the melt will be higher at the time of initiation of flooding. The use of larger applied transients will also be explored.

#### 2.4.3 Effect of the Mode of Pressure Transient Introduction

The sequence of experiments initiated last quarter to investigate the effect of the mode of pressure-transient introduction into the hot-liquid/cold-liquid system was continued. In each of the experiments performed this quarter, the pressure transient was introduced into the melt without involving the water by the method in which a projectile moving at velocities of 50 m/s strikes the stainless-steel rod projecting from the bottom of the hearth.<sup>5</sup> This method was used because it was shown to be the most effective method tried in the preliminary experiments. The projectile velocities were measured as described in the previous report by causing the projectile to sequentially clip a pair of current-carrying fine wires which were threaded through two pairs of vent holes in the end of the inverted gun barrel (see Figure 2.1.2 of Reference 4). As also reported previously, pressure transients of the order of 1 MPa in magnitude and 50  $\mu$ s in duration were produced in static water at the normal sample location with this method.



Five through-the-hearth experiments (numbers 9-125-1 through 9-129-2 in Table III) were performed in the current series with the pressure transients applied from 0.05 to 0.27 s after flooding was initiated. The known explosive, oxidic Corium-E simulant with 61.5 at/o initial oxygen content, was used for the series. Initial melt temperatures ranged from 1931 to 2094 K; flooding water had temperatures between 287 and 294 K. Not even coarse fragmentation of the melt occurred for these experiments, although it did occur for the single previously reported experiment (9-124-1) using this method of pressure transient introduction.

To eliminate the possibility that the particular batch of oxidic Corium-E simulant material used in the through-the-hearth triggering experiments was somehow different from previous batches, a control experiment (9-130-1) was performed in which a sample of the same batch was melted in argon, flooded with room-temperature water, and subjected to a bridgewire-generated transient in the standard through-the-water method. A two-stage fragmentation and pressure-generating interaction occurred, just as in the previous experiments of that type.

There is still concern that the through-the-hearth pressure pulses which are measured in static water just above the hearth at the sample location in the test experiments are not necessarily representative of the transients seen by the molten sample in an actual triggering experiment. The fact that a small amount of typical fragmentation debris, part of which was in the form of spherules in the 30- to 60- $\mu\text{m}$ -dia range, was produced in the one similar experiment performed last quarter (9-124-1) suggests that the pressure transients introduced by this method may be marginal for triggering the interaction. At present, therefore, it is felt that the experiments performed to date neither prove nor disprove the ability of through-the-hearth pulses to initiate steam explosions. Further experiments are being designed to remove this uncertainty.

## 2.5 Debris Analyses

The analyses of debris produced by the interaction of highly oxidized corium-E simulants with water were extended this quarter. Effort in that area was confined mainly to scanning electron microscopy of the various fractions obtained by sieving the residue retrieved from experiment 9-102-1. That experiment, as previously reported,<sup>5</sup> produced a 1.47-MPa pressure pulse in the second stage of the interaction which occurred approximately 6 ms after the application of the bridgewire pulse. The initial oxygen content of the Corium-E simulant used in that experiment was 62.5 atom percent.

From Figure 8, which is a corrected version of Figure 11 of Reference 5, it can be seen that the debris from Experiment 9-102-1 was separated into seven fractions extending from the residue which passed through a screen with 45- $\mu\text{m}$ -dia openings to the residue which was retained on a sieve with 850- $\mu\text{m}$ -dia openings. The peak of the mass lay in the fraction which was retained on the 45- and passed through 75- $\mu\text{m}$  sieves.

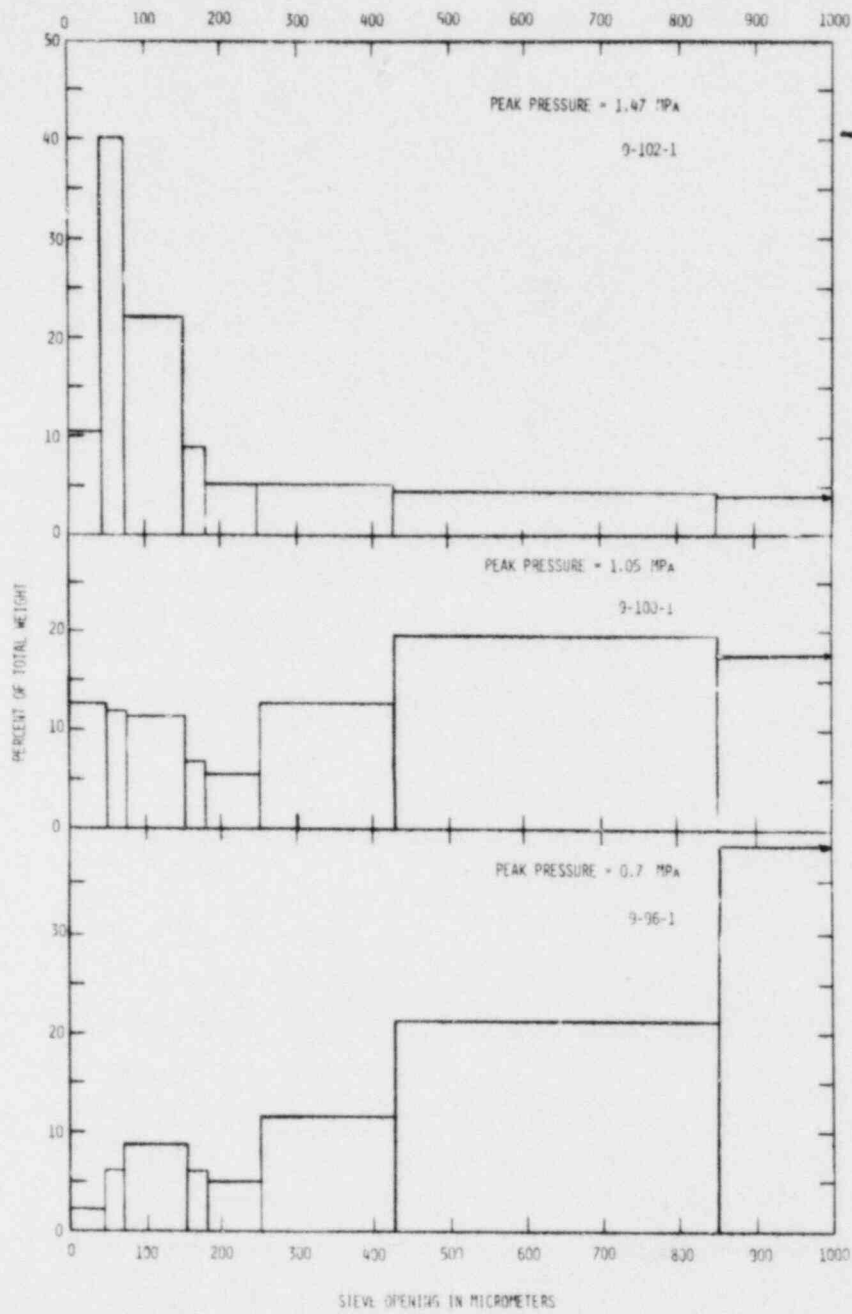


Figure 8. Weights of Various Sieve Fractions for Three Corium-E Samples

Scanning electron microscopy was performed on the three smaller diameter sieve fractions: through the 45- $\mu\text{m}$ , through the 75- $\mu\text{m}$ , and caught on the 45- $\mu\text{m}$ ; and through 150- $\mu\text{m}$  and caught in the 75- $\mu\text{m}$  sieves. Typical scanning electron micrograph images of these fractions are shown in Figure 9.

It is noteworthy that the smaller size fractions shown in Figure 9 contain only a few spheroidal particles. Most of the particles have mossy or shard-like morphologies. (But, as reported last quarter, both the spheroid and mossy morphologies have identical metal atom compositions, as shown by in situ EDAX analyses in the microscope during imaging.)

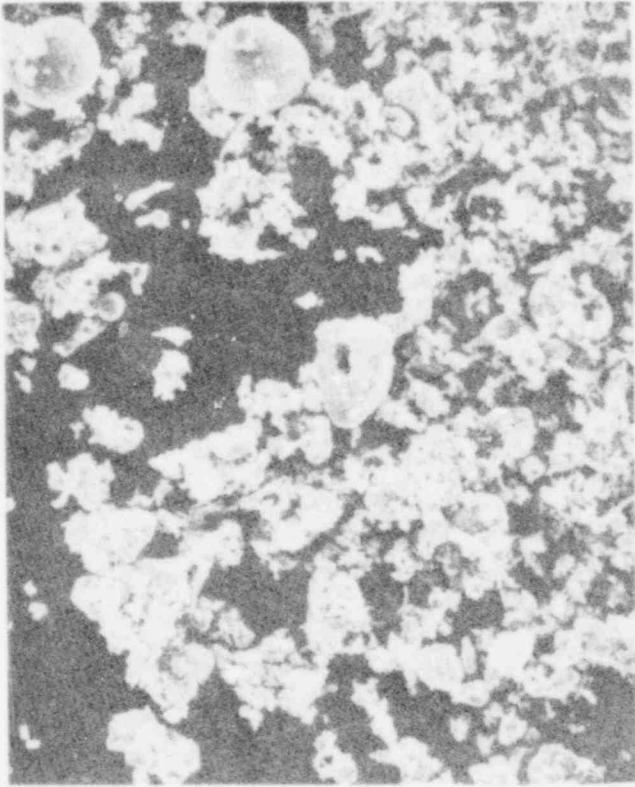
A few of the larger particles were also examined. A particle from the next to largest fraction (through the 850- $\mu\text{m}$  but caught on the 425- $\mu\text{m}$  sieve) is shown in Figure 10. Only a few spheroidal particles were also found in the fractions which contain the largest particles. Most particles were unmelted artifacts.

Since there were few spheroidal particles in either the largest or the smallest size fractions, it can be concluded that if there are significant quantities of spheroidal particles in the debris from Experiment 9-102-1, they must be predominantly in the intermediate sieve fractions (150- to 425- $\mu\text{m}$ -dia fractions).

A few particles from the 150/75- and 75/45- $\mu\text{m}$  sieve fractions were examined at higher magnification for unusual or interesting structures. Images from these particles are shown in Figures 11 and 12, respectively. Little interpretation of these images has been attempted as yet, except to note that dendritic crystal growth has been observed in some of the structures. By determining the interdendritic spacings, it is possible to estimate the cooling rates of the individual particles.<sup>11</sup>

Further studies of debris are being planned in which specimens will be cross sectioned by polishing and examined again by scanning electron microscopy techniques. An attempt will also be made to determine the phase structures of the particles by electron diffraction techniques.

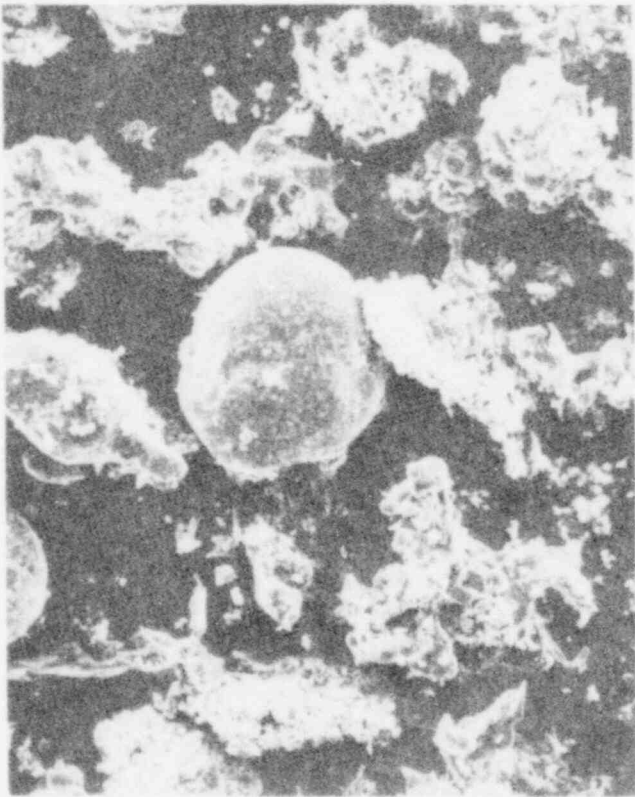
Scanning electron micrographs were also taken of the small amount of debris produced in Experiment 9-124-1, an interaction between 61.5 a/o initial oxygen-containing Corium-E simulant and water initiated by a through-the-hearth pressure transient.<sup>5</sup> Images of the debris produced are shown in Figure 13. Although there are a number of particle morphologies, there are many spheroidal particles. Their similarity to the debris generated in the bridgewire experiments suggests that possibly a small degree of interaction was, in fact, triggered by the through-the-hearth pulse.



(a)



(b)



(c)

Figure 9.

Typical Scanning Electron Micrographs of Sieved Debris from the Interaction of Corium-E Simulant (62.5 Atom Percent Oxygen Initially) Which Had Been Flooded With 295 K Water and Subjected to a Bridgewire Pulse 0.14 Sec Later. All Material in (a) passed through a sieve with 45- $\mu\text{m}$  openings. Material in (b) passed through a sieve with 75- $\mu\text{m}$  openings and was caught on one with 45- $\mu\text{m}$  openings. Material in (c) passed through a sieve with 150- $\mu\text{m}$  openings and was caught on one with 75- $\mu\text{m}$  openings (9-102-1). Horizontal width of each photo is 0.57 mm.

POOR ORIGINAL

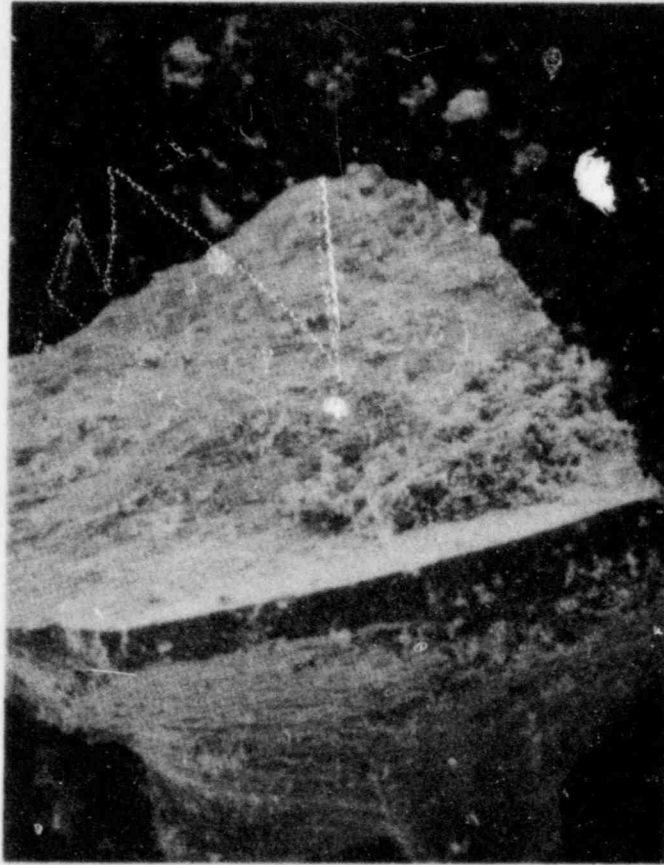
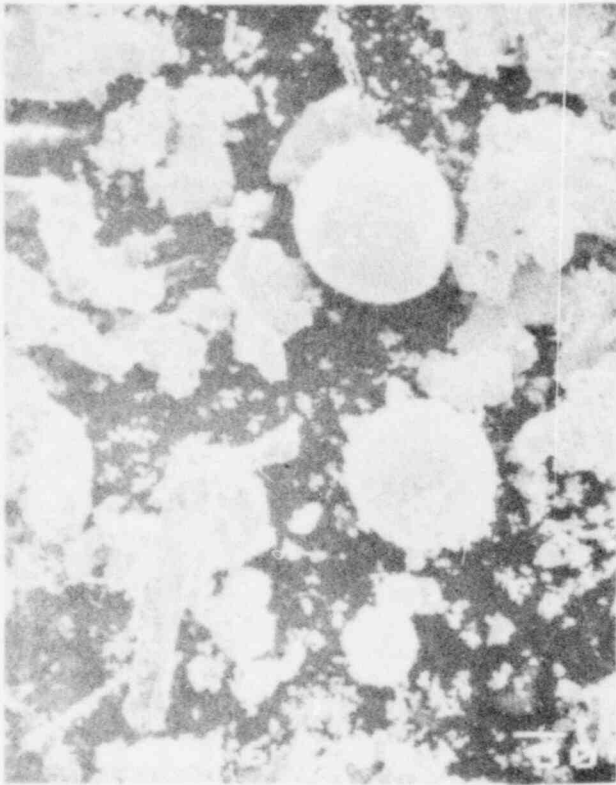
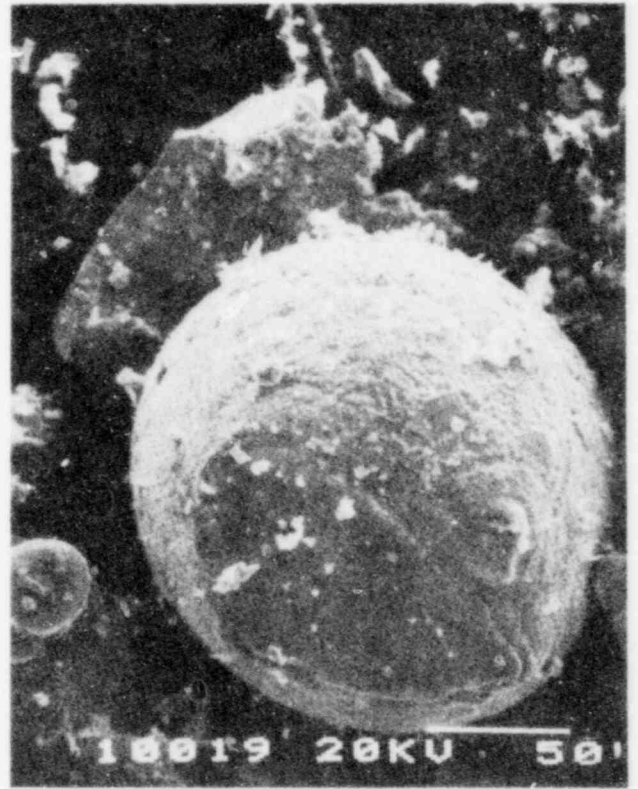


Figure 10. A Scanning Electron Micrograph of a Piece of Sieved Debris from the Interaction of Corium-E Simulant (62.5 atom percent oxygen initially) Which Had Been Flooded with 295 K Water and Subjected to a Bridge-wire Pulse 0.14 Sec Later. Sample is part of the material which had passed through a sieve with 850- $\mu\text{m}$  openings and was caught on a sieve with 425- $\mu\text{m}$  openings (9-102-1). Horizontal width of photo is 0.57 mm.

POOR ORIGINAL



(a-1). Bar is 50  $\mu\text{m}$  long.



(a-2). Bar is 50  $\mu\text{m}$  long.



(a-3). Bar is 5  $\mu\text{m}$  long.

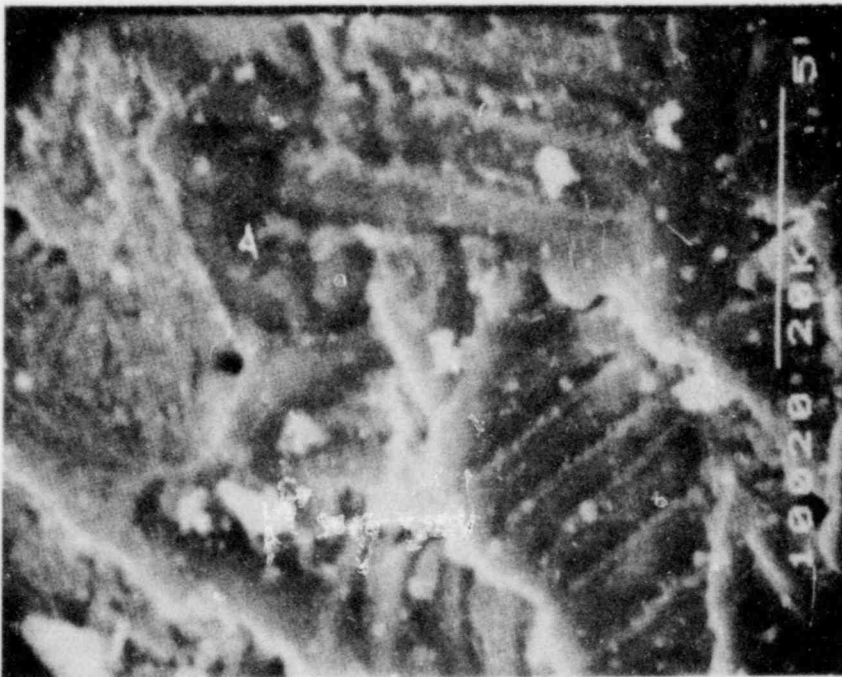
Figure 11(a).

Another Portion of the Fraction Shown in Figure 9(c). Spheroid at upper center in (a-1) is shown in increasing magnifications in successive images (9-102-1).

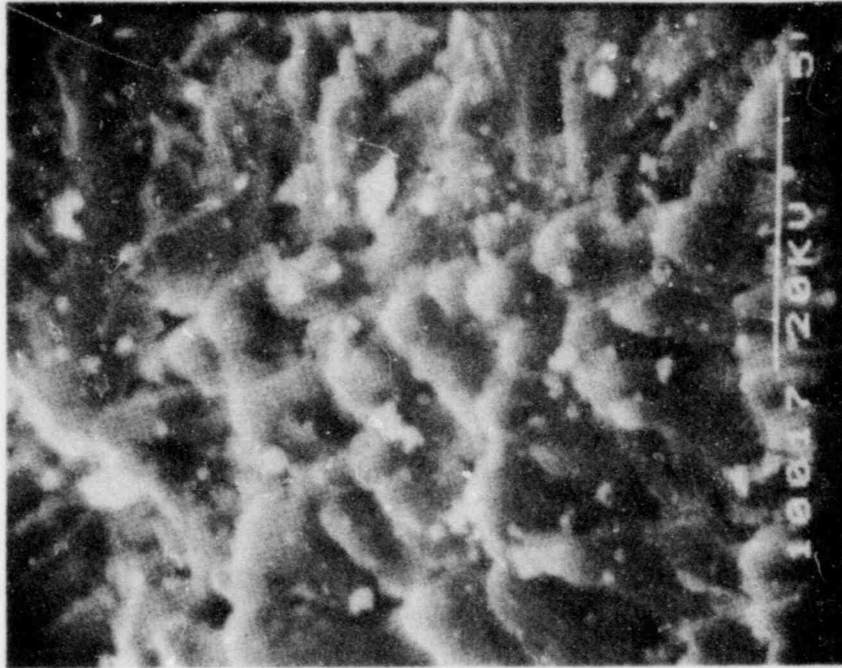
Figure 11.

Particles from the fraction Shown in Figure 9(c)

POOR ORIGINAL

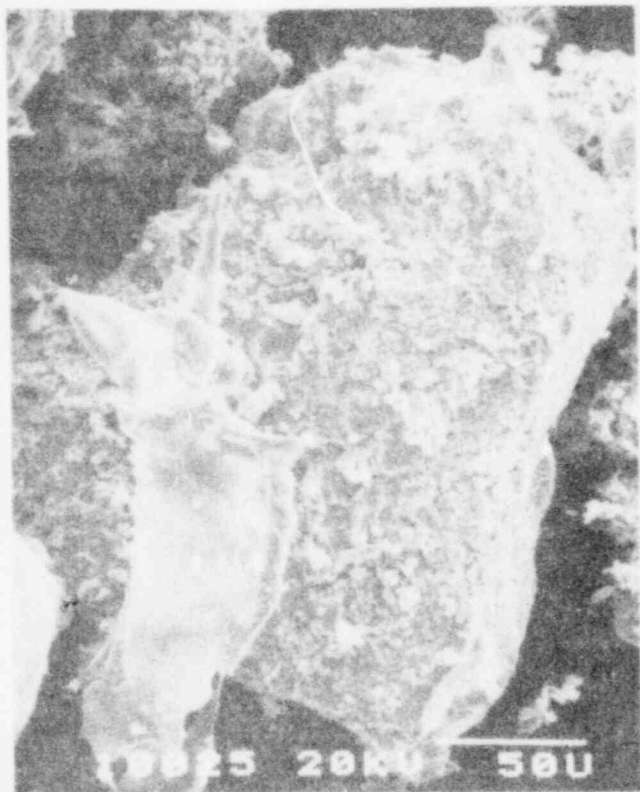


(a-4). Bar is 5  $\mu$ m long.



(a-5). Bar is 5  $\mu$ m long.

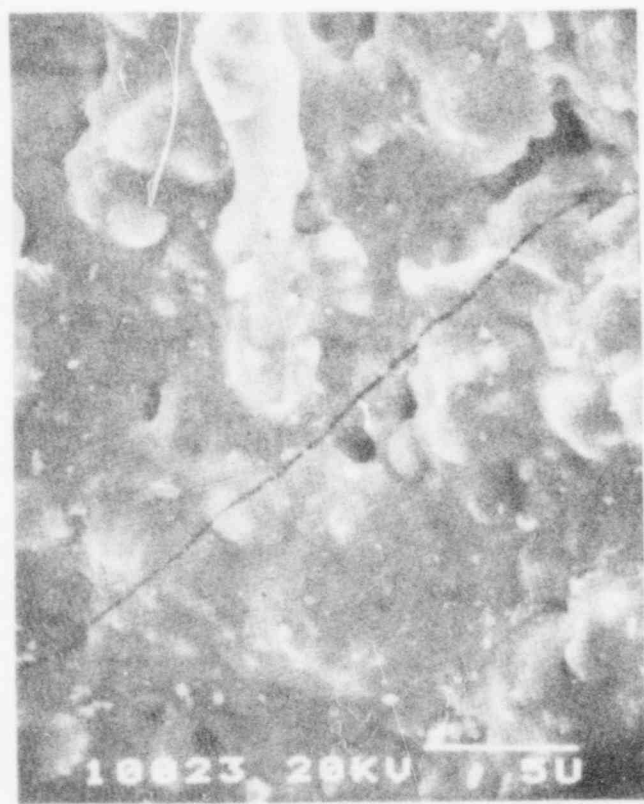
Figure 11(a). (Concluded)



(b-1). Bar is 50  $\mu$ m long.



(b-2). Bar is 50  $\mu$ m long.



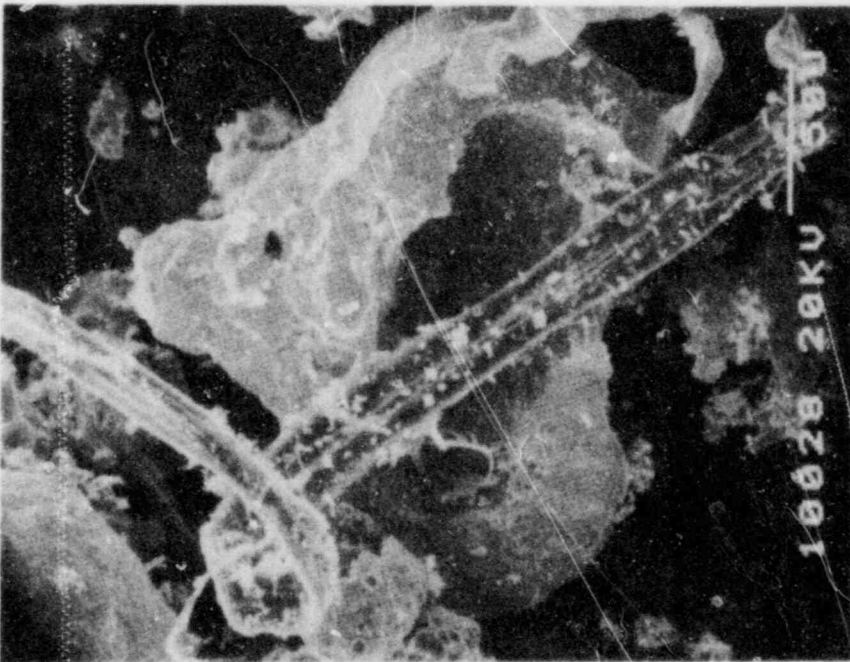
(b-3). Bar is 5  $\mu$ m long.

Figure 11(b).

Another Portion of the  
Fraction Shown in Figure  
9(c), at Increasing  
Magnifications.

POOR ORIGINAL





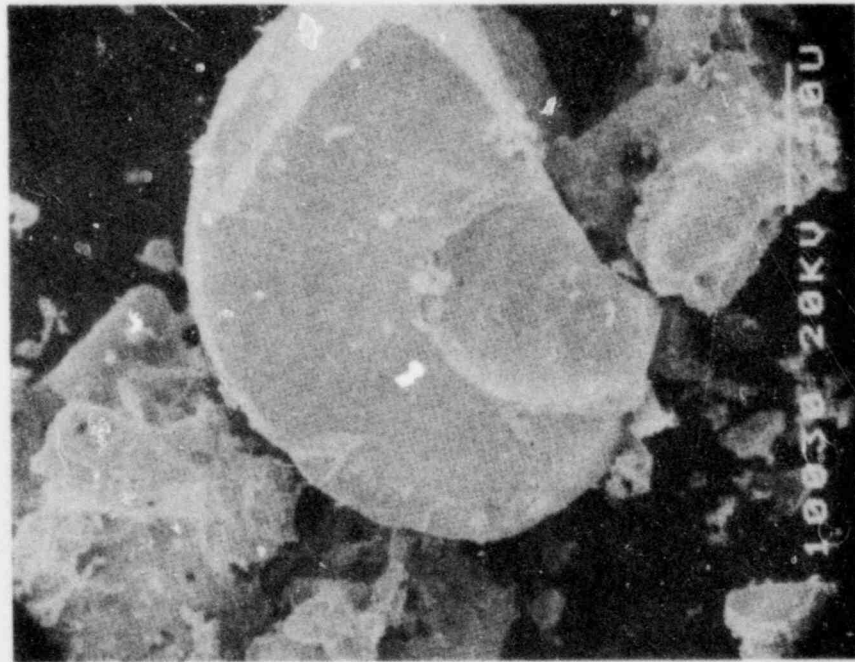
(c-1). Bar is 50  $\mu$ m long.



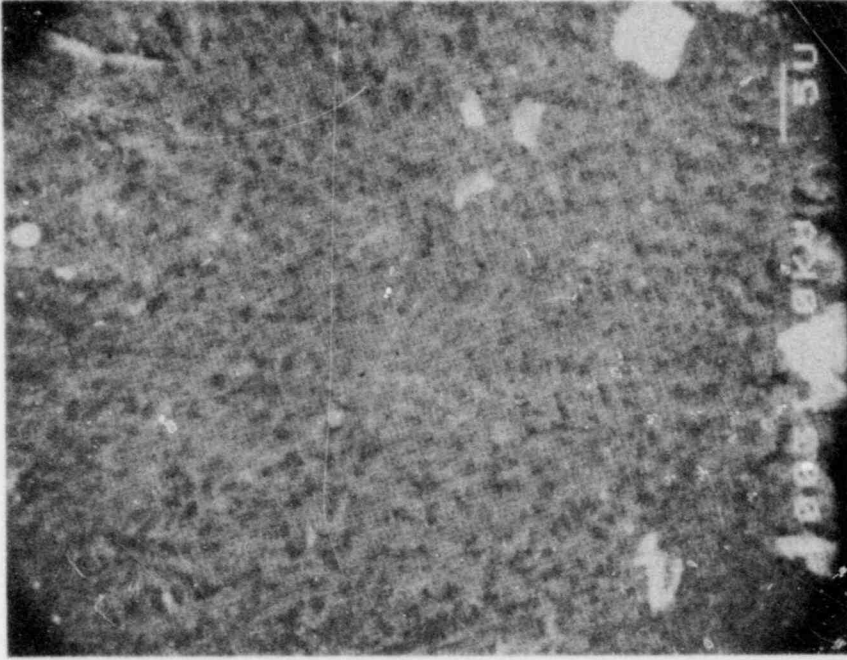
(c-2). Bar is 5  $\mu$ m long.

Figure 11(c). Another Portion of the Fraction Shown in Figure 9(c), at Increasing Magnifications

POOR ORIGINAL

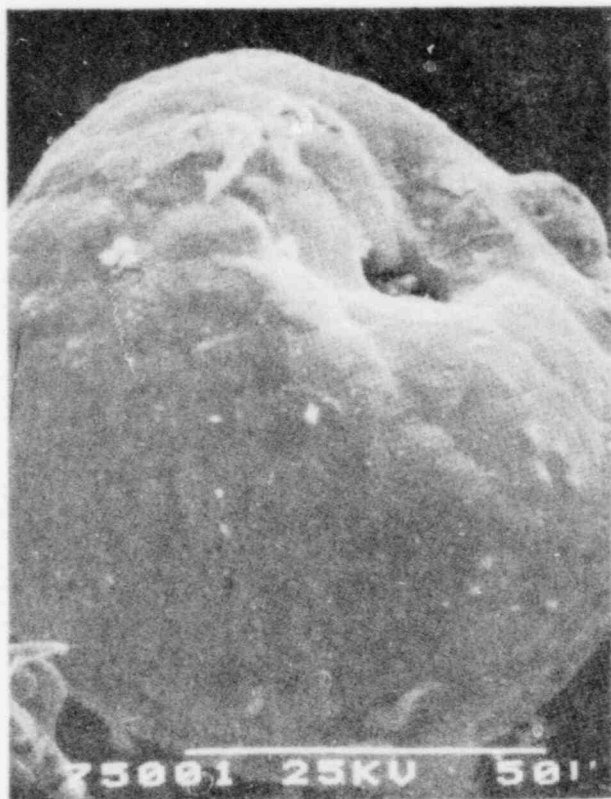


(d-1). Bar is 50  $\mu\text{m}$  long.

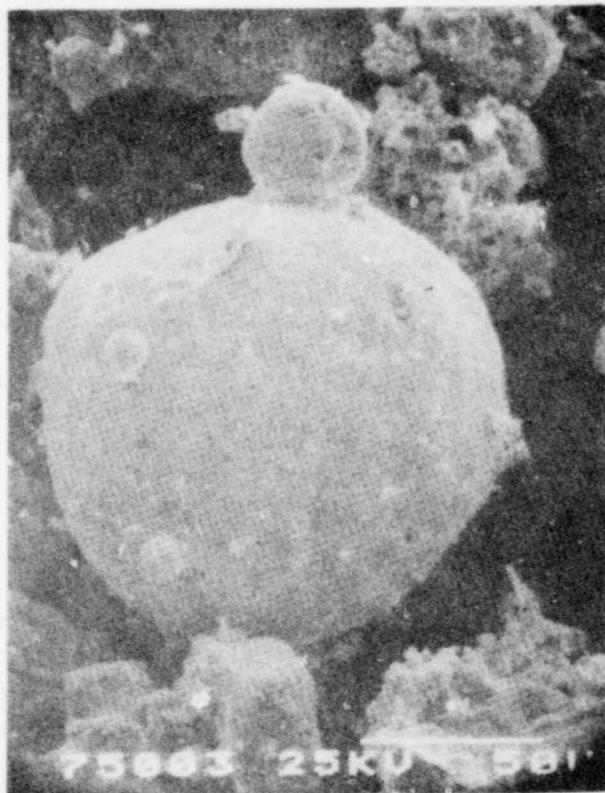


(d-2). Bar is 5  $\mu\text{m}$  long.

Figure 11(d). Another Portion of the Fraction Shown in Figure 9(c), at Increasing Magnifications



(a). Bar is 50  $\mu\text{m}$  long.



(b-1). Bar is 50  $\mu\text{m}$  long.



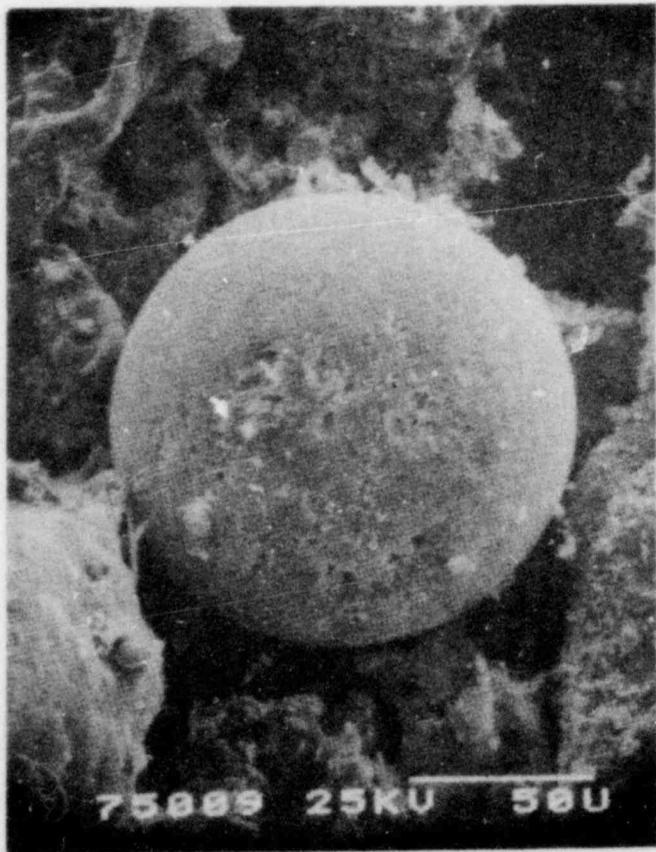
(b-2). Bar is 5  $\mu\text{m}$  long.  
(Some dendritic growth is visible in the originals.)

Figure 12.

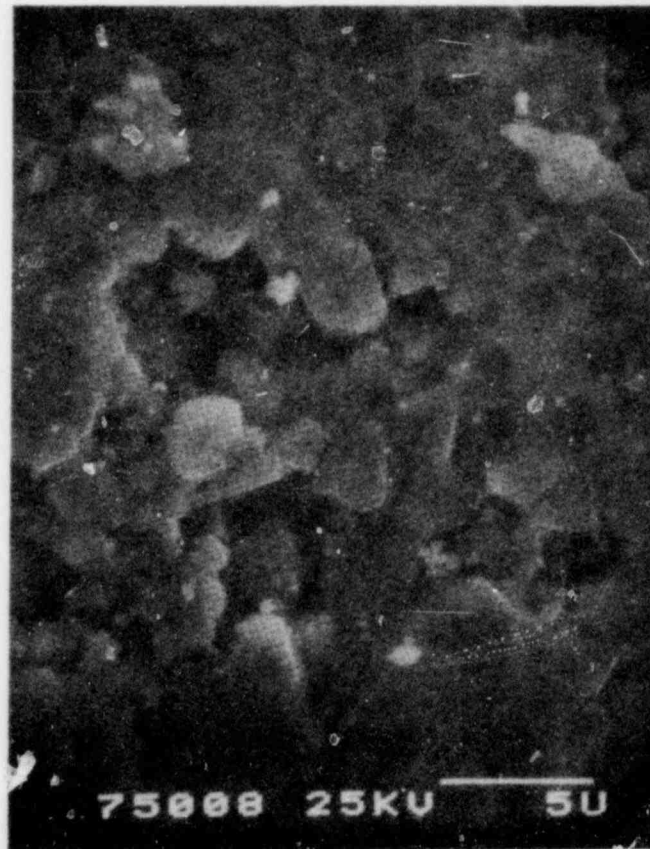
Particles from the Fraction Shown  
in Figure 9(b). In (b) through  
(d), two magnifications are shown.

POOR ORIGINAL

POOR ORIGINAL



(c-1). Bar is 50  $\mu\text{m}$  long.



(c-2). Bar is 5  $\mu\text{m}$  long.

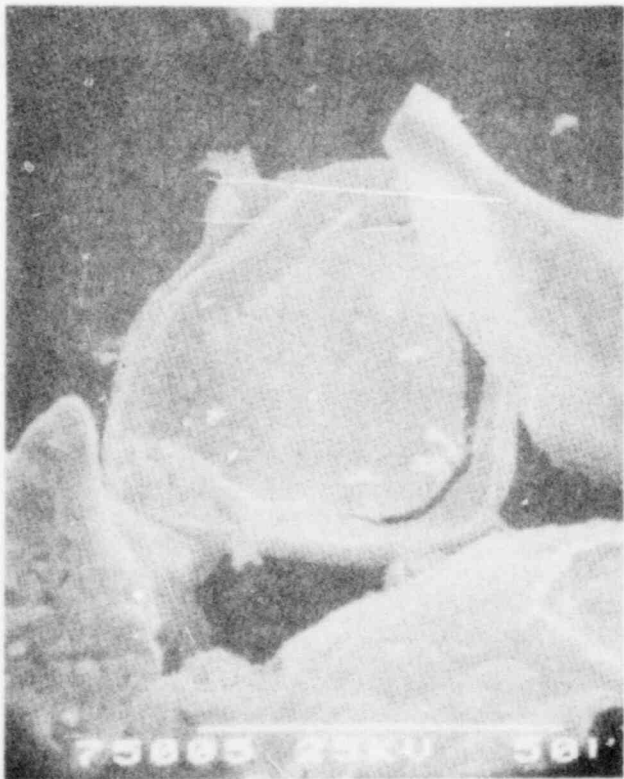
Figure 12. (Continued)



(d-1). Bar is 50  $\mu\text{m}$  long.



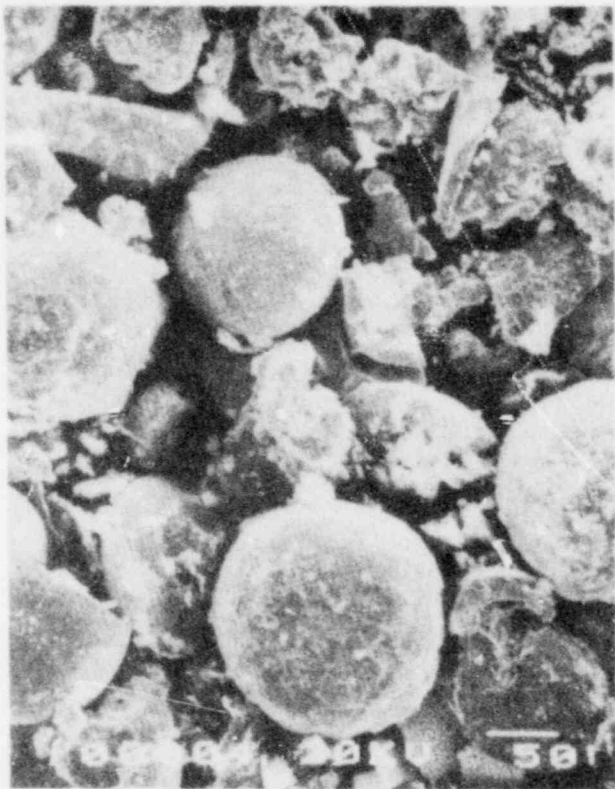
(d-2). Bar is 5  $\mu\text{m}$  long.



(e). Bar is 50  $\mu\text{m}$  long.

Figure 12. (Concluded)

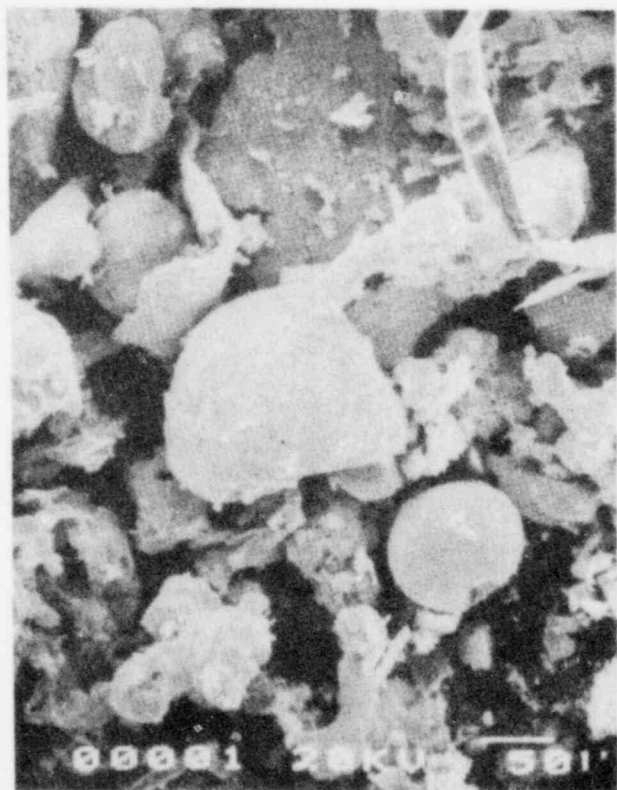
POOR ORIGINAL



(a)



(b)



(c)

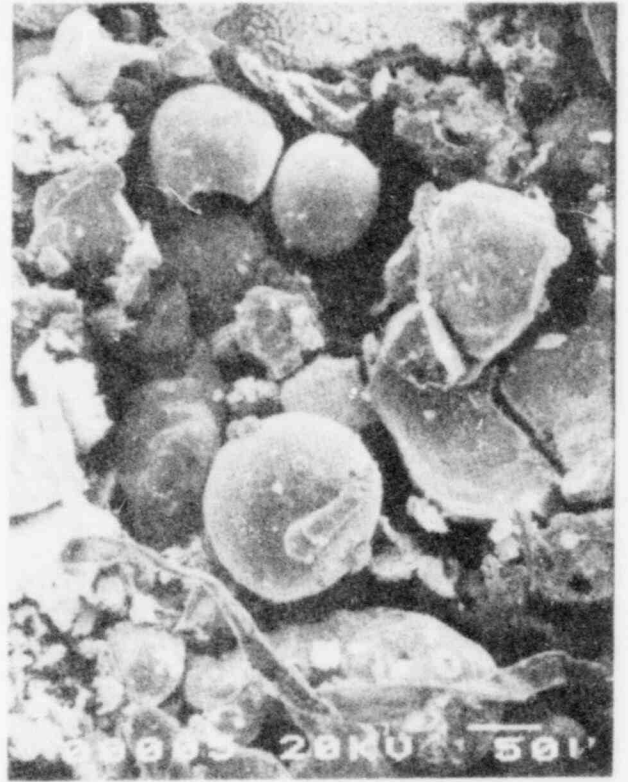
Figure 13.

Scanning Electron Micrographs of As-Retrieved Debris Produced When Molten Corium-E Simulant, 61.5 a/o Initial Oxygen Content, was Flooded with Water and Exposed to a Through-the-Hearth Pressure Transient (9-124-1). In each micrograph, bar is 50  $\mu\text{m}$  long.

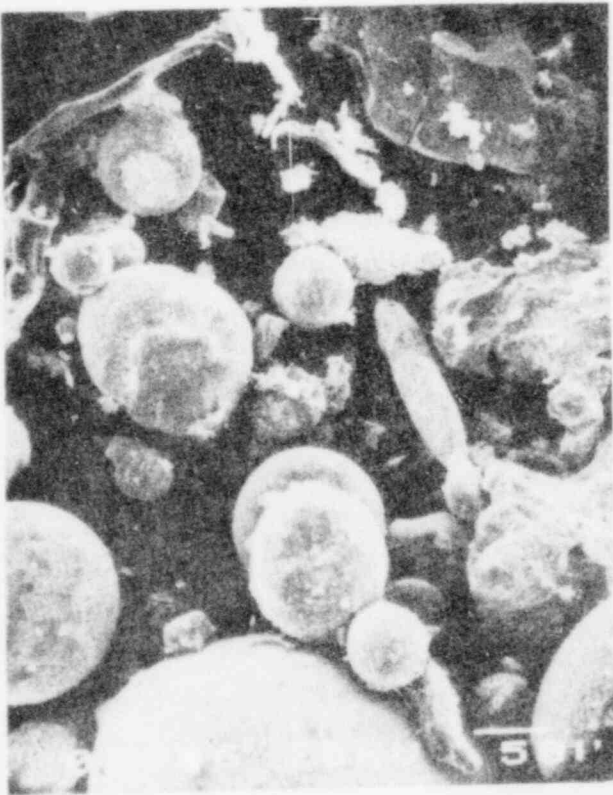
POOR ORIGINAL



(d)



(e)



(f)

Figure 13. (Concluded)

POOR ORIGINAL

## 2.6 Exploratory Melting Experiments

Two exploratory melting experiments with a fully oxidic Corium-A simulant (58.3 w/o  $\text{UO}_2$ , 20.9 w/o  $\text{ZrO}_2$ , 20.8 w/o  $\text{Fe}_2\text{O}_3$ ; composition calculated from the metal atom ratios of Peehs<sup>9</sup>) resulted in what appears to be a one-phase liquid which froze in argon in a well-behaved manner. Globules were obtained which are similar to the argon-frozen globules produced with the fully oxidic Corium-E simulant. A photograph of a sample (9-131-1) of oxidic Corium-A simulant frozen in argon is shown in Figure 14. No floodings of Corium-A compositions were attempted this quarter.

A similar attempt to arc-melt pure uranium dioxide was disappointing. It was not possible to achieve significant quantities of melt, and the pellet which was being heated showed a concave, glassy, interior lining, quite similar to the experiments performed with the metallic Corium-E simulant. In addition to the incomplete melting, there was copious evolution of vapor which produced large quantities of aerosol in the chamber and much wall deposition. A photograph of the sample on which melting was attempted is shown in Figure 15. (Note the similarity to the sample of metallic Corium-E simulant shown in Figure 19 of Reference 10.)

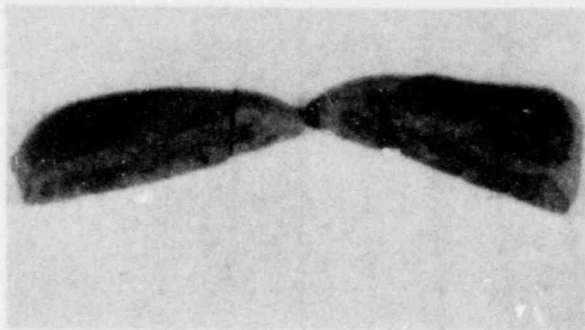


Figure 14. Photograph of a Cross-Sectioned Sample of Oxidic Corium-A Simulant Which Had Been Arc-Melted and Frozen in Argon (9-131-1). Grid is 6.4 mm.

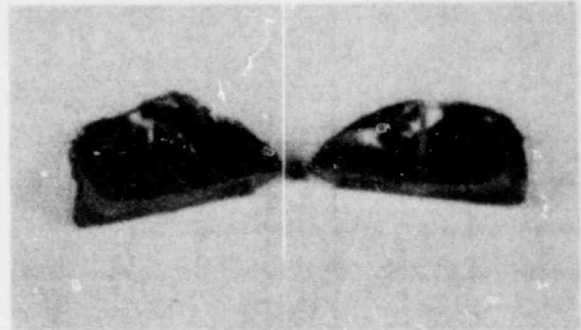


Figure 15. Photograph of a Cross-Sectioned Sample of Uranium Dioxide Which Had Been Subjected to Arc Heating and Then Frozen in Argon (9-131-1). Grid is 6.4 mm.

## 2.7 Containment Breaching Analysis

Two previous quarterly reports<sup>5, 10</sup> contained discussions on the molten-core/water-contact analysis which has been performed as one task of the fiscal year 1977 steam-explosion phenomena program. That task is intended to address one portion of the probability of containment damaging steam explosions occurring during a hypothetical core-melt accident, specifically the probability of large amounts of molten core materials contacting similar amounts of water. The triggering experiments address another portion of the containment breaching question: the probability of any steam explosion occurring. The efficiency scaling studies will address a third portion: the prob-

POOR ORIGINAL



ability of explosions which might occur being sufficiently efficient and large enough to actually fail the containment building. The containment breaching probability also involves identifying a containment failure mechanism, which is the topic of this section.

For in-vessel explosions, the Reactor Safety Study analysis model<sup>12</sup> assumed that the failure was caused by the reactor vessel head being blown through the containment building roof. No credit was taken in that analysis for the energy dissipated in crushing any structures encountered in traversing the considerable distance to the roof. Neither was any credit taken for the amount of energy required to penetrate the roof. Only gravitational forces were considered. Since a considerable amount of energy can be expended in penetrating nearly 3 ft of reinforced concrete, a crude analysis was performed to compare a typical vessel head and control rod structure kinetic energy value (based on the Reactor Safety Study containment breaching analysis) with the amount of energy needed to shear a plug from the containment roof. That analysis indicated the projectile had approximately the right amount of energy needed to penetrate but, as with the Reactor Safety Study analyses, no credit was taken here either for the crushing of the control rod drive mechanism. On the other hand, the analysis assumed that a full 50-ft-dia hole had to be punched in the roof which is probably unrealistic since a smaller diameter hole could possibly yield similar high-release consequences. Unless a much more elaborate explosion model and structural model are combined and they indicate otherwise, it seems valid to assume, from a structural point of view at least, that the reactor head can indeed be given sufficient energy in a large, efficient steam explosion to cause containment breaching.

Concern has also been given to the probability that smaller missiles might cause containment breaching for steam explosions involving much less molten-core material. For that reason, analyses have also been performed investigating the penetrability requirements of projectiles like rods and pipes. These were performed using a typical empirical ballistic penetration formula developed for low-velocity missiles. The analyses indicated that the thermal energy contained in only a few hundred pounds of molten-core material would be more than sufficient to allow a reasonably large hole to be made in the containment walls or roof. The difficulty in evaluating these small projectiles as a threat to containment integrity, however, lies in determining where such projectiles would physically originate in the accident situation and how the steam-explosion energy would be effectively coupled to them. No reasonable scenarios have yet been determined.

## 2.8 Steam Explosion Scaling Studies

The planning of a program to investigate the effects of size scaling on the efficiency of thermal interactions between molten-core materials and water was continued this quarter. The main contribution to that area was the preparation of a "need and scope" document for the scaling program. That document was issued in draft form during the quarter.<sup>8</sup> Its preparation entailed a literature review to ensure that the latest available information on scaling had been considered as well as communication with known investigators planning or performing a large-scale experiments.

All available data on thermal interactions of two liquids involving 1 kg or greater quantities of molten metals or oxides as the hot liquid were reviewed for possible application to the scaling problem. All available theories and models pertaining to scaling were also reviewed to determine their applicability to the LWR accident analysis. The summary results of that document are given below.

The most important question about steam explosions in a hypothetical fuel-melt accident is whether relatively small triggering disturbances can grow through thermal interaction into large-scale, efficient, destructive explosions when molten light-water reactor core components contact water. There presently is no basis for believing this cannot happen since current theoretical explanations do not prohibit it, and very little applicable data are available to suggest otherwise. Qualitative data are available for other systems which suggest that efficient interactions might be possible. Therefore, an investigation of scaling is required for simulated LWR fuel-melt accident conditions.

The scaling program experiments should primarily attempt, with good diagnostic procedures, to obtain the time dependence of thermal to mechanical energy conversion efficiencies for simple, large-scale (1 to 25 kg) steam explosions. A secondary goal of the scaling program should be to investigate the physical processes occurring during triggering and propagation, but the configurations and diagnostic procedures should not be chosen to specifically optimize that portion. The program should also provide for as complete an analysis of the data as possible in terms of all the various theories.

It could perhaps be argued that the scaling studies should not be performed since several similar large-scale programs are already in progress. Unfortunately, those programs each seem to lack at least one important element in addressing the efficiency question for molten LWR core materials. The main deficiencies are that the programs are either designed for the study of inappropriate materials or do not include the possible use of artificial triggers. These two elements are considered to be sufficiently important to justify an additional program.

## References

1. Light Water Reactor Safety Research Program Quarterly Report July - September 1975, SAND75-0632, Nuclear Fuel Cycle Safety Research Department, Sandia Laboratories, Albuquerque, New Mexico, Dec, 1975.
2. D. A. Dalgran, Ed., Light Water Reactor Safety Research Program Quarterly Report April - June 1976, SAND76-0677, Sandia Laboratories, Albuquerque, New Mexico, Feb, 1977.
3. Light Water Reactor Safety Research Program Quarterly Report January - March 1976, SAND76-0369, Nuclear Fuel Cycle Safety Research Department, Sandia Laboratories, Albuquerque, New Mexico, Sept, 1976.
4. Light Water Reactor Safety Research Program Quarterly Report October - December 1975, SAND76-0163, Nuclear Fuel Cycle Safety Research Department, Sandia Laboratories, Albuquerque, New Mexico, April 1976.
5. Light Water Reactor Safety Research Program Quarterly Report January - March 1977, SAND77-1249, Nuclear Fuel Cycle Safety Research Department, Sandia Laboratories, Albuquerque, New Mexico, Oct, 1977.
6. L. S. Nelson and L. D. Buxton, Trans. Am. Nucl. Soc., 26, 397 (1977).
7. L. D. Buxton and L. S. Nelson, Trans. Am. Nucl. Soc., 26, 398 (1977).
8. L. D. Buxton, Effect of Size Scaling on Steam Explosion Energy Conversion Efficiency, ROUGH DRAFT, Org. 5412, Sandia Laboratories, Albuquerque, New Mexico, June 9, 1977.
9. M. Peehs, Investigations of Molten Corium Phases, International Atomic Energy Authority Report No. IAEA-SM-190/10, Kraftwerk Union Aktiengesellschaft, Erlangen, Germany, pp. 355-368, 1975.
10. Light Water Reactor Safety Research Program Quarterly Report October - December 1976, SAND77-0944, Nuclear Fuel Cycle Safety Research Department, Sandia Laboratories, Albuquerque, New Mexico, July 1977.
11. P. A. Joly and R. Mehrabian, J. Mat. Sci., 9, 1446 (1974).
12. W. A. Carbiener et al., U. S. Nuclear Regulatory Commission, Reactor Safety Study, An Assessment of Accident Risks in U. S. Commercial Nuclear Power Plants, Appendix VIII, WASH-1400, NUREG-75/014, Oct, 1975.

DISTRIBUTION:

U. S. Nuclear Regulatory Commission  
(356 copies for R3)  
Division of Document Control  
7920 Norfolk Avenue  
Bethesda, Maryland 20014

Dr. M. Fisher  
Gesellschaft für Kernforschung  
Project Nuclear Safety (PNS)  
75 Karlsruhe  
Postfach 3640  
Federal Republic of Germany

Dr. H. Albrecht  
Gesellschaft für Kernforschung  
PNS/IRCH  
75 Karlsruhe  
Postfach 3640  
Federal Republic of Germany

Dr. J. P. Hosemann  
Gesellschaft für Kernforschung  
Project Nuclear Safety  
75 Karlsruhe  
Postfach 3640  
Federal Republic of Germany

Professor of Mayinger  
Lehrstuhl and Institut für  
Verfahrenstechnik  
T. U. Hannover  
3000 Hannover 1  
Callinstr. 15 F  
Federal Republic of Germany

Milad Matthias  
Department of Nuclear Studies  
and Safety  
Ontario Hydro  
700 University Avenue (H-16)  
Toronto, Ontario  
Canada M5G1X6

Gesellschaft für Kernforschung (2)  
PNS/RBT  
75 Karlsruhe  
Postfach 3640  
Federal Republic of Germany  
Attn: Dr. S. Hagen  
D. Perinic

Dr. H. Holleck  
Gesellschaft für Kernforschung  
PNS/IMF  
75 Karlsruhe  
Postfach 3640  
Federal Republic of Germany

H. Seipel  
BMFT  
Federal Ministry for Research  
and Technology  
53 Bonn  
Federal Republic of Germany

Dr. E. Herkommer  
Institute for Reactor Safety  
5000 Köln 1  
Gloschengasse 2  
Federal Republic of Germany

Professor Dr. H. Unger, IKE  
University of Stuttgart  
7 Stuttgart-Vaihingen  
Pfaffenwaldring 31  
Federal Republic of Germany

W. B. Murfin, PNS  
Gesellschaft für Kernforschung  
75 Karlsruhe  
Postfach 3640  
Federal Republic of Germany

G. H. Kinchin  
Safety and Reliability Directorate  
Wigshaw Lane  
Culcheth  
NR Warrington, Cheshire  
England

Dr. M. Peehs, KWU  
Abt. Rb. 3  
852 Erlangen  
Postfach 325  
Federal Republic of Germany

Dr. M. Dalle Donne (2)  
Kernforschungszentrum Karlsruhe  
Institut für Neutronenphysik  
und Reaktortechnik  
75 Karlsruhe 1  
Postfach 3640  
Federal Republic of Germany

Dr. H. Kottowski  
c/o - Euratom Ispra  
21020 Centro Euratom di Ispra  
(Varese) Italy

Dr. Rudolf Benz (2)  
Dr. George Froehlich, IKE  
7 Stuttgart 80  
Pfaffenwaldring 31  
Federal Republic of Germany

DISTRIBUTION (cont'd)

Division of Reactor Safety Research (8)  
Office of Nuclear Regulatory Research  
U. S. Nuclear Regulatory Commission  
Mail Station: G158  
Washington, DC 20555

Attn: M. Silberberg, Chief  
Experimental Fast Reactor Safety Br.  
R. W. Wright, Experimental Fast  
Reactor Safety Branch  
R. DiSalvo, Fuel Behavior Research Branch (6)

U. S. Department of Energy (4)  
Reactor Safety Research Coordination  
Washington, DC 20545  
Attn: R. W. Barber, Actg. Director (3)  
T. E. McSpadden, Project Manager

U. S. Department of Energy  
Operational Safety Division  
Albuquerque Operations Office  
P. O. Box 5400  
Albuquerque, New Mexico 87115  
Attn: J. R. Roeder, Director

Argonne National Laboratory (2)  
9700 South Cass Avenue  
Argonne, Illinois 60439  
Attn: H. H. Hummel  
R. E. Henry

Oak Ridge National Laboratory  
Box Y, Building 9201-3  
Oak Ridge, Tennessee 37830  
Attn: M. H. Fontana

Brookhaven National Laboratory  
Upton, Long Island, New York 11973  
Attn: W. Y. Kato, Head  
Fast Reactor Safety Division

University of California (2)  
Energy and Kinetics Department  
5530 Boelter Hall  
Los Angeles, California 90024  
Attn: W. E. Kastenberg  
J. N. Castle

Idaho National Engineering Laboratory  
EG&G Idaho, Inc.  
P. O. Box 1625  
Idaho Falls, Idaho 83401  
Attn: A. W. Cronenberg

University of Arizona (2)  
Department of Nuclear Engineering  
Tucson, Arizona 85721  
Attn: R. L. Seale  
R. L. Brehm

Westinghouse Advanced Reactor Division  
P. O. Box 158  
Madison, PA 15663  
Attn: L. E. Strawbridge

Dr. H. Mizuta, PNC  
Oarai Engineering Center  
4002 Narita, Oarai-Machi  
Ibaraki-Ken  
Japan

Offshore Power Systems  
8000 Arlington Expressway  
P. O. Box 8000  
Jacksonville, FL 32211  
Attn: D. H. Walker  
Nuclear Safety & Licensing

400 C. Winter  
1200 L. D. Smith  
Attn: K. J. Touryan, 1260  
T. B. Lane, 1280  
1261 D. O. Lee  
1262 H. C. Hardee  
1262 D. W. Larson  
5000 A. Narath  
5131 W. B. Benedick  
5160 W. Herrmann  
5163 H. J. Sutherland  
5167 B. M. Butcher  
5167 J. E. Smaardyk  
5216 K. L. Goin  
5333 B. D. Zak  
5333 L. S. Nelson  
5400 A. W. Snyder  
5410 D. J. McCloskey  
5411 D. A. Dahlgren  
5411 M. Berman  
5411 L. D. Buxton (10)  
5411 R. K. Cole  
5411 R. L. Knight  
5412 J. W. Hickman  
5420 J. V. Walker  
5422 R. L. Coats  
5422 H. G. Plein  
5423 J. E. Powell  
5423 G. A. Carlson  
5425 W. J. Camp  
5430 R. M. Jefferson  
5450 J. R. Reuscher  
5830 M. J. Davis  
5831 N. J. Magnani  
5831 T. M. Gerlach  
5831 D. A. Powers  
5831 R. S. Sallach  
5833 F. J. Zanner  
5846 E. K. Beauchamp  
9330 A. J. Clark, Jr.

DISTRIBUTION (cont's)

9337 N. R. Keltner

8266 E. A. Aas

3141 T. L. Werner (5)

3151 W. L. Garner (3)

For DOE/TIC (Unlimited Release)

DOE/TIC (25)

(R. P. Campbell, 3172-3)

UNITED STATES  
NUCLEAR REGULATORY COMMISSION  
WASHINGTON, D. C. 20555

OFFICIAL BUSINESS  
PENALTY FOR PRIVATE USE, \$300

POSTAGE AND FEES PAID  
U.S. NUCLEAR REGULATORY  
COMMISSION



POOR ORIGINAL